Bull. Disas. Prev. Res. Inst., Kyoto Univ., Vol. 41, Part 3, No. 359, September, 1991

Transverse Mixing in a River with Complicated Channel Geometry

By Yoshiaki IWASA and Shirou AYA

(Manuscript received on Sept. 30, 1991; revised on Nov. 26, 1991)

Abstract

This paper investigates the flow behavior and the associated mixing in a river system with complicated geometry by means of two-dimensional numerical analysis. The basic mathematical models for flows and mixing in the generalized curvilinear coordinate system are derived from the usual equations for shallow water in the Cartesian coordinate system, and the numerical models with use of FDM is developed. The models are applied to the Yodo River System which has three main tributaries; flow behavior and concentration distributions at/below the confluence of the Yodo River System are obtained, and they are successfully compared with the observed data.

The characteristics of flow behavior and the transverse mixing at/below the confluence of the Yodo River System are also investigated by both numerical and simplified physical experiments under various hydraulic conditions. The characteristics may be summarized as follows: 1) The distribution of the river bed elevation is non-uniform in the longitudinal and the transverse directions. Therefore, the transverse distribution of the momentum flux vector varies in the longitudinal direction, 2) This variation makes the convective transport of concentration in the transverse direction, with the convection having more dominant roles in transverse mixing than the dispersion transport, 3) Therefore, the concentration distribution is much influenced by the discharge condition and the river bed topography. These features are also demonstrated by our simplified physical model study.

1 Introduction

1.1 Objectives

It is common for effluents from sewerage systems to be discharged into rivers, whereby the water quality in a receiving river is usually worse than in the upstream part of a river. When river waters are the source of potable water, the water quality problem in receiving rivers is serious, and the analysis of spreading of the effluent by use of refined models is required from the point of view of water quality as well as of quantity.

Effluent/contaminants discharged into a river spread in the longitudinal, the transverse and the vertical directions by convection and turbulent transport. The flow in a river is uni-directional and the magnitude of the longitudinal dimension is much greater than in other two directions, so that one-dimensional models have been the most usable. In case the transverse distribution of the concentration is of interest, depth-averaged two-dimensional models are required. The stream tube model by Yotsukura and Sayre[1] is one of the most famous 2-D models and is successfully applied to the analyses of transverse mixing in many river channels[2),3),4)].

It is well known that the hydrodynamic transport processes, that is, convection plays

an important part in mixing in the river, so that 2-D models for flow and the mixing are required in case the flow field is not simple or unsteady, while the contaminant itself is passive. The development of the electronic computer system and software over the last two decades makes these analyses possible and the 2-D mathematical models in the Cartesian coordinate system have mostly been used and solved by the Finite Difference Method (FDM) or Finite Element Method (FEM).

During the last decade, numerical analysis by use of the mathematical models in the curvilinear coordinate system with FDM has been developed, so that it saves computer resources and makes the handling of the computation codes much easier, especially in the flow analysis in complicated domains. A river confluence forms such complicated domains, and this paper will show the 2-D mathematical models for flow behavior and associated mixing in a river in the generalized curvilinear coordinate system, and investigate the flow behavior and the mechanism of the mixing in the actual river system.

1.2 Yodo River System

The area selected in the study is the Yodo River System, which is one of the most important rivers in the Kinki metropolitan area of Japan. Its river and water system are respectively illustrated in **Figs. 1** and **2**. Its river basin is roughly divided into four portions, that is, the three sub-river basins of its three main tributaries: the Uji River, the

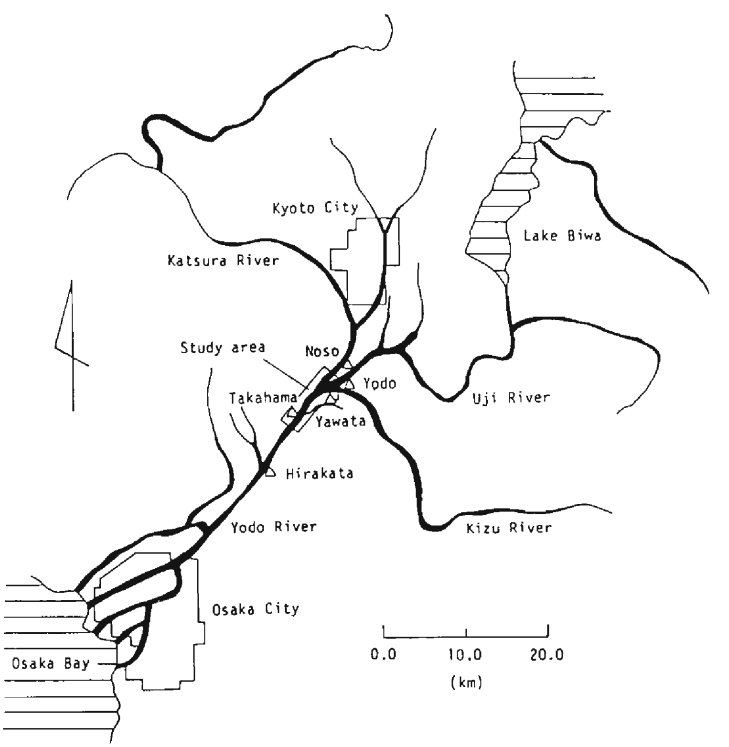

Fig. 1. The Yodo River System.

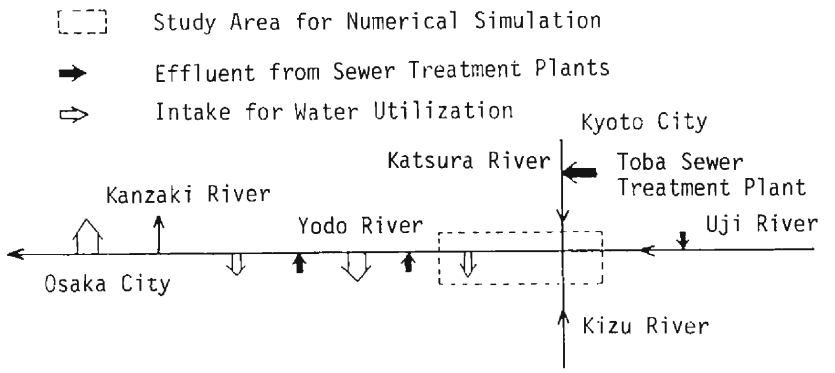

Fig. 2. Outline of water system in the Yodo River Basin.

Table 1. Flow regimes in the Yodo River Sysyem (as of 1980)

Regime	Discharge (m^3/s)			
	Katsura R.	Uji River	Kizu River	Total
Annual average	62.(19.3)	203.(63.2)	56.(17.5)	321.
Ordinary water (185-day) discharge	50.(20.2)	160.(64.5)	38.(15.3)	248.
Low water (275-day) discharge	35.(20.6)	108.(63.5)	27.(15.9)	170.
Drought (355-day) discharge	30.(24.4)	75.(61.0)	18.(14.6)	123.

Figures in the parentheses denote the ratio to total discharge in percentage.

Kizu River and the Katsura River, and the sub-river basin from the confluences of these three tributaries to the river mouth.

The flow regimes in the Yodo River as of 1980 are listed in **Table 1.** The main tributary, the Uji River shares more than 60% to the total amount in discharge throughout all of the flow regimes. In the flow regimes of the annual average, the respective discharge of the Kizu River and the Katsura River is nearly equal to $60 m^3/s$ or about 20% each of the total discharge. This share varies as the total discharge is decreased, because the discharge of the Katsura River includes the constant effluent from the sewer treatment plants in Kyoto City, which is estimated to be about $5 m^3/s$.

Water quality in the Yodo River System is not bad in general; water in the Uji River is relatively clean and it has the highest flow rate amongst the three tributaries. The Kizu River has the highest water quality amongst them because the population in its sub-river basin is small, and water quality in the upstream part of the Katsura River is clean but it worsens just above the confluence of the Yodo River System, because it receives the waste water discharged from Kyoto City. In the lower river basin from the confluence, the Osaka metropolitan area has been developed and the amount of the service water tapping this lower reach is more than $40 m^3/s$, which is distributed to more

than 10 million inhabitants in the metropolitan area. In short, water used in the upstream region from the confluence flows back into the Yodo River, causing water quality problems to the water utilization of the downstream region.

Since the 1950's, much research and field measurements have been undertaken because of the importance of the Yodo River and the scientific interest in the mixing below the confluence. At present, the most convenient method for investigating the water quality in the Yodo River System has been mathematical simulation. The mathematical models are required to express the complicated geometry of the confluence, flow behavior and associated dispersion. The models described in the curvilinear coordinate system will satisfy the above requirements.

2 2-D Numerical Modeling of Flow and Mixing in the Yodo River System

2.1 2-D Numerical Models in the Curvilinear Coordinate System

(1) 2-D Mathematical Models

The basic hydraulic principles applied to describing the flow behavior and the associated mixing of varying concentrations are the conservation laws of momentum, water and mass of dispersion materials. The length scale in the depth-wise direction is much smaller than that in the transverse and the longitudinal directions in rivers, and, therefore, the time scale of mixing is much smaller in the depth-wise direction than in other two directions. As long as the river water is not stratified, the concentration distribution in the depth-wise direction is commonly almost uniform, so that 2-D mathematical models in the horizontal plane are applicable.

Basic 3-D mathematical models for turbulent shear flow and concentration mixing described in the Cartesian coordinate system are:

Momentum equations,

$$\frac{\partial \bar{u}_i}{\partial t}+\frac{\partial \bar{u}_i\bar{u}_j}{\partial x_j}=F_i-\frac{1}{\bar{\rho}}\frac{\partial \bar{p}}{\partial x_i}+\frac{1}{\bar{\rho}}\frac{\partial \overline{\tau_{ij}}}{\partial x_j} \qquad (i, j=1, 2, 3) \tag{1}$$

Continuity equation,

$$\frac{\partial \bar{u}_i}{\partial x_i}=0 \tag{2}$$

Turbulent diffusion equation:

$$\frac{\partial \bar{c}}{\partial t}+\frac{\partial \bar{u}_i\bar{c}}{\partial x_i}=\frac{\partial \bar{s}_i}{\partial x_i} \tag{3}$$

where $\bar{u}_i$ is the ensemble average of velocity in the x_i direction, $\bar{p}$ the ensemble average of pressure, $\bar{\rho}$ the ensemble average of density of water, F_i the body force in the x_i direction, $\overline{\tau_{ij}}$ the x_i directional shear stress acting on the control surface element perpendi-

cular to the x_j direction caused by turbulent motion, $\bar{c}$ the ensemble average of concentration, $\bar{s}_i$ the x_i component of the gradient type mass transport vector caused by turbulent motion, x_i the Cartesian coordinate $(i=1, 2, 3)$, x_1, x_2 the horizontal coordinate respectively, x_3 the vertical coordinate, and t the time. (Hereafter, $^-$(overbars) denoting the ensemble averaged values will be neglected.)

2-D mathematical models are obtained by integrating each of the basic 3-D partial differential equations of Eqs. 1 to 3 from the bottom z_b to the water surface ζ, assuming hydrostatic pressure distribution. Their procedures are well-known and the final results in the Cartesian coordinate system are written as:

$$\frac{\partial}{\partial t}\begin{pmatrix} M_1 \\ M_2 \\ h \\ N \end{pmatrix}+\frac{\partial}{\partial x_i}\begin{pmatrix} U_iM_1 \\ U_iM_2 \\ U_ih \\ U_iN \end{pmatrix}=\frac{\partial}{\partial x_i}\begin{pmatrix} h\tau'_{1i}/\rho \\ h\tau'_{2i}/\rho \\ 0 \\ hS_i \end{pmatrix}+\begin{pmatrix} -gh\cdot\partial\zeta/\partial x_1 \\ -gh\cdot\partial\zeta/\partial x_2 \\ 0 \\ 0 \end{pmatrix}+\begin{pmatrix} -\tau'_{1b}/\rho \\ -\tau'_{2b}/\rho \\ 0 \\ 0 \end{pmatrix} \qquad (i=1, 2) \qquad (4)$$

and

$$U_i\equiv\int_{z_b}^{\zeta}\bar{u}_i dx_3/h \qquad (h=\zeta-z_b) \qquad (5)$$

$$M_i\equiv\int_{z_b}^{\zeta}\bar{u}_i dx_3=U_ih \qquad (6)$$

$$C\equiv\int_{z_b}^{\zeta}\bar{c}dx_3/h \qquad (7)$$

$$N\equiv\int_{z_b}^{\zeta}\bar{c}dx_3 \qquad (8)$$

$$\frac{\tau'_{ij}}{\rho}\equiv-\frac{1}{h}\left\{\int_{z_b}^{\zeta}\overline{(u_i-\bar{u}_i)(u_j-\bar{u}_j)}\,dx_3+\int_{z_b}^{\zeta}(\bar{u}_i-U_i)(\bar{u}_j-U_j)\,dx_3\right\} \qquad (9a)$$

$$\frac{\tau'_{ij}}{\rho}=\nu'\left(\frac{\partial U_i}{\partial x_j}+\frac{\partial U_j}{\partial x_i}\right) \qquad (9b)$$

$$\frac{\tau_{ib}}{\rho}\approx\frac{gn^2M_i\sqrt{M_1^2+M_2^2}}{h^{7/3}} \qquad (10)$$

$$S_i\equiv-\frac{1}{h}\left\{\int_{z_b}^{\zeta}\overline{(c-\bar{c})(u_i-\bar{u}_i)}\,dx_3+\int_{z_b}^{\zeta}(\bar{c}-C)(\bar{u}_i-U_i)\,dx_3\right\} \qquad (11a)$$

$$S_i\equiv D_{ij}\partial C/\partial x_j \qquad (11b)$$

$$(D_{ij})=\begin{pmatrix} D_{11} & D_{12} \\ D_{21} & D_{22} \end{pmatrix}=\begin{pmatrix} \cos^2\theta D_L+\sin^2\theta D_T & \sin\theta\cos\theta(D_L-D_T) \\ \sin\theta\cos\theta(D_L-D_T) & \sin^2\theta D_L+\cos^2\theta D_T \end{pmatrix} \qquad (12)$$

where U_i is the x_i component of the depth-averaged velocity vector, M_i the x_i component of the momentum flux vector, h the water depth $(=\zeta-z_b)$, ζ the water surface eleva-

tion, z_b the bottom elevation, C the depth-averaged concentration, N the depth-integrated concentration, τ'_{ij} the x_i directional shear stress acting on the control surface element perpendicular to the x_j direction and it includes the turbulent and dispersion effects, ν' the viscosity coefficient including turbulent and dispersion effects, τ_{ib} the x_i component of the frictional shear stress acting on the bottom, n Manning's roughness coefficient, S_i the x_i component of the gradient type mass transport vector including the turbulent diffusion and the dispersion, D_L the longitudinal dispersion coefficient, D_T the transverse dispersion coefficient, and θ the angle between the Cartesian coordinates and the principal axes of diffusion and dispersion. Eq. 10, equivalent to Manning's formula for 1-D flows, Eq. 9b for the shear stress, and Eq. 11b for the gradient type mass transport are all used in the mathematical models. The definition sketch of variables, and the Cartesian coordinate systems are shown in **Fig. 3.**

Viviand[5] shows the transformation of the conservation form equation; Eq. 13 in the Cartesian coordinate system x_i can be transformed into Eq. 14 in the generalized curvilinear coordinate system ξ_i.

$$\frac{\partial f}{\partial t}+\frac{\partial F_i}{\partial x_i}=0 \qquad (i=1,\ 2,\ 3) \tag{13}$$

$$\frac{\partial}{\partial t}\left(\frac{f}{J}\right)+\frac{\partial}{\partial \xi_i}\left(\frac{f}{J}\frac{\partial \xi_i}{\partial t}+\frac{\partial \xi_j}{\partial x_i}\frac{F_i}{J}\right)=0 \qquad (i,\ j=1,\ 2,\ 3) \tag{14}$$

where ξ and the transformation Jacobian J are respectively defined:

$$\xi_i=\xi_i(x_1,\ x_2,\ x_3,\ t) \qquad (i=1,\ 2,\ 3) \tag{15}$$

$$J\equiv\frac{\partial(\xi_1,\ \xi_2,\ \xi_3)}{\partial(x_1,\ x_2,\ x_3)} \tag{16}$$

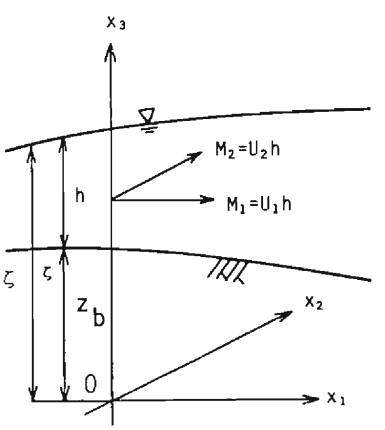

Fig. 3. Definition sketch of variables and the Cartesian coordinate systems.

Hereafter, it is assumed that the new coordinate system (ξ_1, ξ_2) is the function of only the horizontal space coordinates (x_1, x_2):

$$\xi_i=\xi_i(x_1, x_2) \qquad (i=1, 2) \tag{17}$$

Therefore, by application of the relationships described above to each component of the set of Eq. 4 in the Cartesian coordinate system, they are rewritten into a set of partial differential equations in the non-orthogonal curvilinear coordinate system as:

$$\frac{\partial}{\partial t}\left(\frac{1}{J}\right)\begin{pmatrix} M_1 \\ M_2 \\ h \\ N \end{pmatrix}+\frac{\partial}{\partial \xi_i}\left(\frac{1}{J}\right)\begin{pmatrix} U^iM_1 \\ U^iM_2 \\ U^ih \\ U^iN \end{pmatrix}$$
$$=\frac{\partial}{\partial \xi_i}\left(\frac{1}{J}\right)\begin{pmatrix} h\tau'^{1i}/\rho \\ h\tau'^{2i}/\rho \\ 0 \\ hS^i \end{pmatrix}+\frac{1}{J}\begin{pmatrix} -gh\cdot\partial\xi_i/\partial x_1\cdot\partial x_1\cdot\partial\zeta/\partial\xi_i \\ -gh\cdot\partial\xi_i/\partial x_2\cdot\partial\zeta/\partial\xi_i \\ 0 \\ 0 \end{pmatrix}+\frac{1}{J}\begin{pmatrix} -\tau_{1b}/\rho \\ -\tau_{2b}/\rho \\ 0 \\ 0 \end{pmatrix} \tag{18}$$

and

$$U^i\equiv\frac{\partial\xi_i}{\partial x_j}U_j \tag{19}$$

$$\tau'^{ij}=\frac{\partial\xi_j}{\partial x_k}\tau'_{ik} \tag{20}$$

By using Eqs. (9b) and (11b), the shear stress τ'_{ij} and the gradient type mass transport S^i can repectively be written:

$$\frac{\tau'_{ij}}{\rho}=\nu'\left(\frac{\partial\xi_k}{\partial x_j}\frac{\partial U_i}{\partial\xi_k}+\frac{\partial\xi_k}{\partial x_i}\frac{\partial U_j}{\partial\xi_k}\right) \tag{21}$$

$$S^i=D^{ij}\frac{\partial C}{\partial\xi_j} \tag{22}$$

$$D^{ij}=\frac{\partial\xi_i}{\partial x_k}\frac{\partial\xi_j}{\partial x_l}D_{kl} \tag{23}$$

The following is noteworthy concerning the set of Eq. 18:

1. The first equation of Eq. 18 is the momentum conservation equation in the x_1 direction, the second one that in the x_2 direction, the third one the continuity equation, and the fourth one, the mass conservation equation for the contaminant.
2. The dependent variables are the same as those in the Cartesian coordinate system,

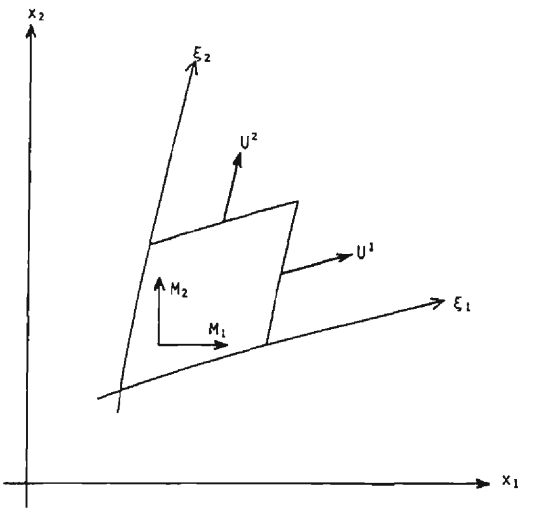

Fig. 4. Cartesian coordinate systems and generalized curvilinear coordinate system.

but only the independent variables are transformed into the non–orthogonal curvilinear coordinate system.

3. They are as simple as those in the Cartesian coordinate system.
4. The new space coordinate system is non–orthogonal curvilinear, by which it is much easier to generate the grids for calculation in the physical domain.

(2) Boundary Conditions

The set of Eq. 18 can be solved under certain boundary and initial conditions. The boundary condition for flows adopted at the closed boundary is the "non–slip condition", for which the following relationship will be specified:

$$M_1=M_2=0 \tag{24}$$

At the open boundary, the distributions of momentum flux vector M or water surface elevation ζ can be specified. In case the distribution of momentum flux vector in the ξ_2 direction is specified, assuming that the coordinate system is orthogonal near the boundary, M_i is obtained as:

$$M_i=\frac{1}{\sqrt{g_{11}}}\frac{\partial x_i}{\partial \xi_1}M^1+\frac{1}{\sqrt{g_{22}}}\frac{\partial x_i}{\partial \xi_2}M^2 \tag{25}$$

where g_{ii} is the metric tensor defined by

$$g_{ii}=\left(\frac{\partial x_1}{\partial \xi_i}\right)^2+\left(\frac{\partial x_2}{\partial \xi_i}\right)^2 \qquad (i=1,\ 2) \tag{26}$$

and M^i the contravariant vector component of momentum flux vector specified. For the usual flow analysis of a river, the measured data of discharge Q is available. Assuming M^2 is equal to zero, M^1 distribution can be obtained as:

$$M_J^1 = Q h_J^{5/3} / \sum_{I=1}^{n} h_I^{5/3} \tag{27}$$

where J denotes the J–th lattice in the ξ_2 direction.

For the conservation equation of concentration, the condition of "no–mass transport" at the closed boundary gives:

$$\frac{\partial C}{\partial \xi_i} = 0 \tag{28}$$

and when the concentration is specified at the upstream open boundary,

$$N = Ch \tag{29}$$

can be used.

(3) Numerical Procedures

The system of the partial differential equations of Eq. 18 can numerically be solved by FDM. The definition points of variables are shown in **Fig. 5** and the finite difference forms of Eq. 18 are obtained by integrating each equation in the hatched or dotted domains in **Fig. 5.** The final finite difference form of each equation of Eq. 18 is obtained by use of Adams–Bashforth scheme for the local derivative, Donor–cell scheme in 2–D plane for convection terms, and the application of the central difference scheme for gradient type transport. The finite difference form of the convective terms usually includes the numerical effects which cause the numerical dispersion and dissipation. The third order finite difference scheme, QUICK[6] and its extension to 2–D phenomena[7], Kawamura's scheme[8] and so on are possible. Iwasa et al[9] showed that the Donor–cell scheme of second order accuracy gives results similar to the QUICK scheme, when the coordinate system is selected in accordance with the flow direction.

The momentum equation in the x_1 direction is written as:

$$\frac{\partial}{\partial t}\left(\frac{\phi}{J}\right) + L_1(\phi) = L_2(\phi) + L_3(\phi) + L_4(\phi) \tag{30}$$

The finite difference representation for each term of Eq. 30 is shown as: The local time derivative term is approximated as

$$\phi^{n+1} \approx \phi^n + J\Delta t\left\{ -\frac{3}{2}L_1(\phi^n) + \frac{1}{2}L_1(\phi^{n-1}) + \frac{3}{2}L_2(\phi^n) - \frac{1}{2}L_2(\phi^{n-1}) \right.$$

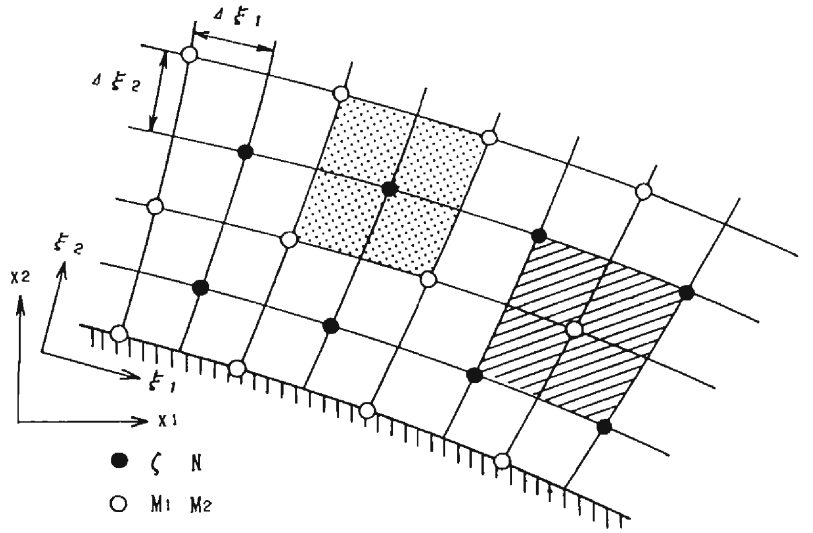

Fig. 5. Definition points of variables and domains for integrating the mathematical models in a physical plane. Open circles denote the points for M_1 and M_2, and solid circles ζ and N. Dotted domain is for the equations for mass and concentration, and hatched domain for the momentum equations.

$$+\frac{3}{2}L_3(\phi^n)-\frac{1}{2}L_3(\phi^{n-1})+\frac{3}{2}L_4(\phi^n)-\frac{1}{2}L_4(\phi^{n-1})\Big\} \tag{31}$$

The convective terms,

$$L_1(\phi)\equiv\frac{\partial}{\partial\xi_i}\Big(\frac{1}{J}U^i\phi\Big) \tag{32a}$$

are approximated as

$$\frac{1}{2\Delta\xi_1 2\Delta\xi_2}\iint L_1(\phi)\,d\xi_1 d\xi_2{}_{I,J}\approx\frac{1}{2\Delta\xi_1 2\Delta\xi_2}\Big\{\int\Big(\frac{U^1}{J}\phi\Big)d\xi_2{}_{I+1,J}-\int\Big(\frac{U^1}{J}\phi\Big)d\xi_2{}_{I-1,J}$$

$$+\int\Big(\frac{U^2}{J}\phi\Big)d\xi_1{}_{I,J+1}-\int\Big(\frac{U^2}{J}\phi\Big)d\xi_1{}_{I,J-1}\Big\} \tag{32b}$$

and

$$\int\Big(\frac{U^1}{J}\phi\Big)d\xi_2{}_{I,J}\approx\frac{1}{J_{I,J}}\frac{1}{2}\{U^1_{I,J}(\phi_{I-1,J}+\phi_{I+1,J})+|\,U^1_{I,J}\,|\,(\phi_{I-1,J}-\phi_{I+1,J})\}2\Delta\xi_2 \tag{32c}$$

$$\int\left(\frac{U^2}{J}\phi\right)d\xi_{1_{I,J}}\approx\frac{1}{J_{I,J}}\frac{1}{2}\{U^2_{I,J}(\phi_{I,J-1}+\phi_{I,J+1})+|U^2_{I,J}|(\phi_{I,J-1}-\phi_{I,J+1})\}2\Delta\xi_1 \tag{32d}$$

Hereafter, subscript I, J and so on denote the variables at the lattice point $(I\Delta\xi_1, J\Delta\xi_2)$ or the center of the integration.

The turbulent and dispersive viscosity terms,

$$L_2(\phi)\equiv\frac{\partial}{\partial\xi_i}\left(\frac{h}{J}\frac{\tau'^{ij}}{\rho}\right) \tag{33a}$$

are approximated as

$$\frac{1}{2\Delta\xi_1 2\Delta\xi_2}\int\int L_2(\phi)\,d\xi_1 d\xi_{2_{I,J}}\approx\frac{1}{2\Delta\xi_1 2\Delta\xi_2}\left\{\left(\frac{h}{J}\frac{\tau'^{i1}}{\rho}\right)2\Delta\xi_{2_{I+1,J}}-\left(\frac{h}{J}\frac{\tau'^{i1}}{\rho}\right)2\Delta\xi_{2_{I-1,J}}\right.$$

$$\left.+\left(\frac{h}{J}\frac{\tau'^{i2}}{\rho}\right)2\Delta\xi_{1_{I,J+1}}-\left(\frac{h}{J}\frac{\tau'^{i2}}{\rho}\right)2\Delta\xi_{1_{I,J-1}}\right\} \tag{33b}$$

The pressure terms,

$$L_3(\phi)\equiv-\frac{gh}{J}\left(\frac{\partial\xi_i}{\partial x_j}\frac{\partial\zeta}{\partial\xi_i}\right)_{I,J} \tag{34a}$$

are approximated as

$$\frac{1}{2\Delta\xi_1 2\Delta\xi_2}\int\int L_3(\phi)\,d\xi_1 d\xi_{2_{I,J}}\approx-g\left(\frac{h}{J}\right)_{I,J}\left\{\left(\frac{\partial\xi_1}{\partial x_j}\right)_{I,J}\frac{1}{2\Delta\xi_1}(\zeta_{I+1,J}-\zeta_{I-1,J})\right.$$

$$\left.+\left(\frac{\partial\xi_2}{\partial x_j}\right)_{I,J}\frac{1}{2\Delta\xi_2}(\zeta_{I,J+1}-\zeta_{I,J-1})\right\} \tag{34b}$$

τ'^{ij} is calculated by the relationship of Eqs. 20 and 21, and the space derivative of the depth averaged velocity can be approximated by the central difference scheme.

The bottom shear-stress term,

$$L_4(\phi)\equiv-\frac{1}{J}\frac{\tau_{ib}}{\rho} \tag{35a}$$

is approximated as

$$\frac{1}{2\Delta\xi_1 2\Delta\xi_2}\int\int L_4(\phi)\,d\xi_1 d\xi_{2_{I,J}}\approx-\left(\frac{1}{J}\frac{\tau_{ib}}{\rho}\right)_{I,J} \tag{35b}$$

In case it is required that the variable not be at its definition points, it may be calculated by linear interpolation.

3 Verification of the Numerical Models

The developed models are applied to the Yodo River System. As stated in **1.2,** it has three main tributaries, each with different flow characteristics and concentration fields. They merge into the Yodo River and the confluence has complicated flow behavior as well as geometry. Although much research and the field measurement on the mixing in the Yodo River System have been made, the hydraulic characteristics of the mixing have not yet been clarified.

3.1 Outline of Simulations for Verification

The segment of the Yodo River System selected for study includes the confluences. Its downstream boundary is 32.0km from the reference point near the river mouth and the upstream boundary 36.2km at the Katsura River, 36.2km at the Uji River, and 0.4km at the Kizu River from its own reference point. (See **Figs. 1** and **6(a)**). The river channels concerned are limited to only low flow channels, because our study focuses on the spreading of the contaminant and the resultant water quality problem is usually serious during the low-flow condition.

The new grid system is generated by use of the geographical survey data in the Yodo River. They include the cross-sectional survey lines and the numerically interpolated ones by Akima's method[10] as shown in **Fig. 6(a)**. Non-orthogonal curvilinear grids of about 25m in length and 5m in width cover the study area of about 4km in length and about 100m in width as illustrated in **Fig. 6(a)**. The selected study area includes two confluences, that is, the Kizu River merging into the Uji River at the upper confluence located at the 35.2km section, and the Katsura River merging into the Uji River at the lower confluence located at the 34.4km section. The non-uniform distribution of river bed elevation and concavities and convexities were observed. There is a big concavity along the right bank side between two confluences and a convexity below the concavity. There are also some concavities along the right or the left bank side below the lower confluence. (See **Fig. 6(b)**.)

The flow discharge and the concentration distribution, i.e., the transverse distributions of the flow rate per unit width and concentration of the contaminants are specified according to the results of the field measurements at the upstream boundaries of the three tributaries. The uniform water surface elevation is also specified at the downstream boundary in the main stream.

The values of the parameters specified in the mathematical models are: Manning's roughness coefficient $n=0.02$, the turbulent and dispersive viscosity coefficient $\nu' = 0.01\,\mathrm{m^2/s}$, the longitudinal dispersion coefficient $D_L = 5.93hu_*$ according to Elder[11], and the transverse dispersion coefficient $D_T = 0.2hu_*$ measured in laboratory[11), 12), 13), 14)], where u_* is the friction velocity defined by $\sqrt{ghI}$. Detailed discussion on the transverse dispersion coefficient in the Yodo River System will be given in **3.2 (4)** and **Section 4.**

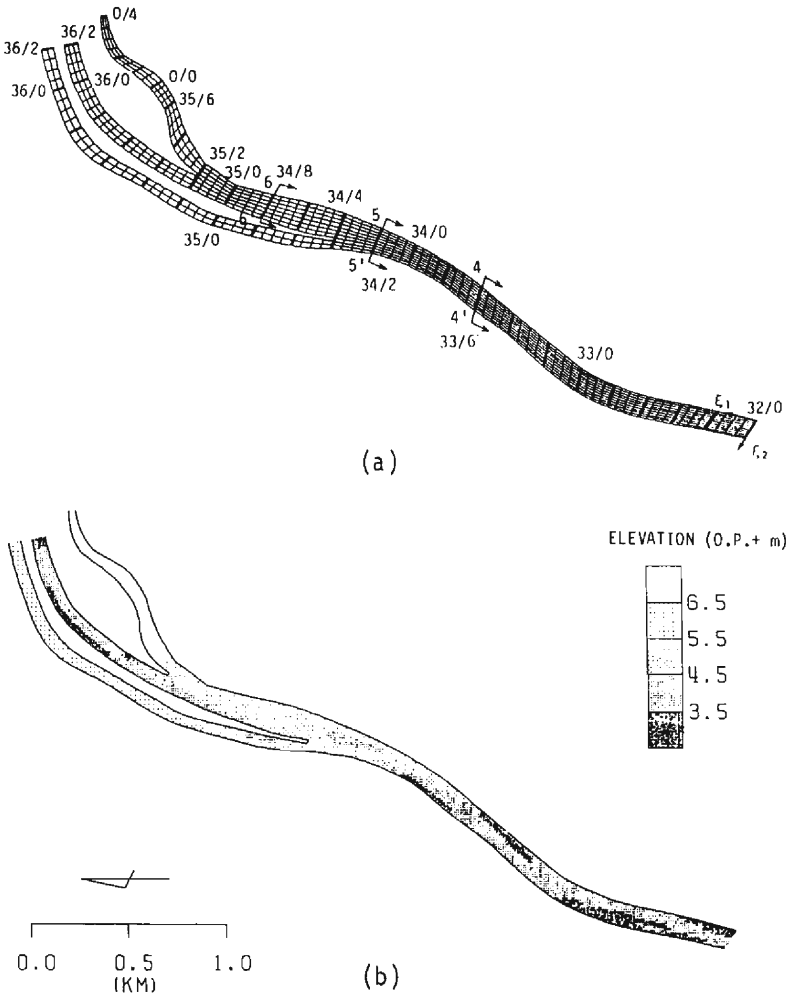

Fig. 6. The Yodo River Confluence selected for study area for (a) Generated curvilinear grids, and (b) bathymetric map (in O. P.+m). The thick solid lines in Fig. (a) indicate the cross-sectional survey lines.

Two sets of verification test, that is, 62–0904 Test and 61–1028 Test were conducted. Field measurements were made in the period of low or drought water discharge, and flow and concentration fields were confirmed to be almost steady-state. 2-D models described in the previous subsections can calculate unsteady behavior of flow and concentration. However, by specifying the steady-state boundary conditions, they give the steady flow and concentration fields, and only the results under the steady conditions will be presented. The specified boundary conditions for two tests are summarized in **Table 2.** The selected water-quality parameters are NH_3–N for 62–0904 Test, and NH_3–N and SiO_2 for

Table 2. Summary of boundary conditions for 62–0904, and 61–1028 Tests

Test	Item		Katsura R.	Uji R.	Kizu R.	Yodo R.
62–0904	Discharge	$Q(m^3/s)$	19.0	120.4	11.2	——
	Stage	ζ(O. P.+m)	——	——	——	5.13
	NH_3–N Conc.	C(mg/l)	3.39	0.24	0.13	——
61–1028	Discharge	$Q(m^3/s)$	18.4	60.5	11.4	——
	Stage	ζ(O. P.+m)	——	——	——	5.75
	NH_3–N Conc.	C(mg/l)	3.03	0.35	0.14	——
	SiO_2 Conc.	C(mg/l)	9.00	2.27	13.21	——

61–1028 Test. The transverse concentration distributions of these water-quality parameters at each upstream boundary section of the three rivers were almost uniform. NH_3–N concentration in the Katsura River is the highest among the three tributaries because it receives the effluent from sewer treatment plants in Kyoto City, but SiO_2 concentration is the highest in the Kizu River.

3.2 Simulation Results and Discussions

(1) Steady-State Flow Behavior

Water surface elevation contour map, the momentum flux vector distributions and the depth-averaged velocity vector distributions obtained in the simulation for 62–0904 Test will be discussed below.

Water surface elevation contour lines are nearly perpendicular to channel boundaries as shown in **Fig. 7(a)**. The decrease of water surface elevation in the lower reach below the second confluence is very small and the water surface profile is shown by backwater curves in a mild slope channel. In the upper reach, the water depth is shallow and the water surface profile is more influenced by the river bed condition; the river bed in the Kizu River is the highest and the extent of the water surface elevation is the greatest. On the contrary the bed-slope in the Uji River is nearly horizontal or partially adverse, so that very small increase of the water surface elevation is obtained. The water surface of the Katsura River lies between other two tributaries, reflecting its river bed slope.

The distributions of the momentum flux vector and depth-averaged velocity vector distributions are shown in **Fig. 7(b)** and **(c)**, respectively. In the upper three segments above each of the confluences, their transverse distributions are nearly uniform, because the river bed elevation in the transverse direction is nearly uniform in the Kizu River and Katsura River, while the water depth in the Uji River is deep. Below the upper confluence, the Kizu River merges into the Uji River. The river bed elevation in the Uji River is much lower than that in the Kizu River, so that the water of the Kizu River flows into the right side of the channel below the upper confluence, and the momentum

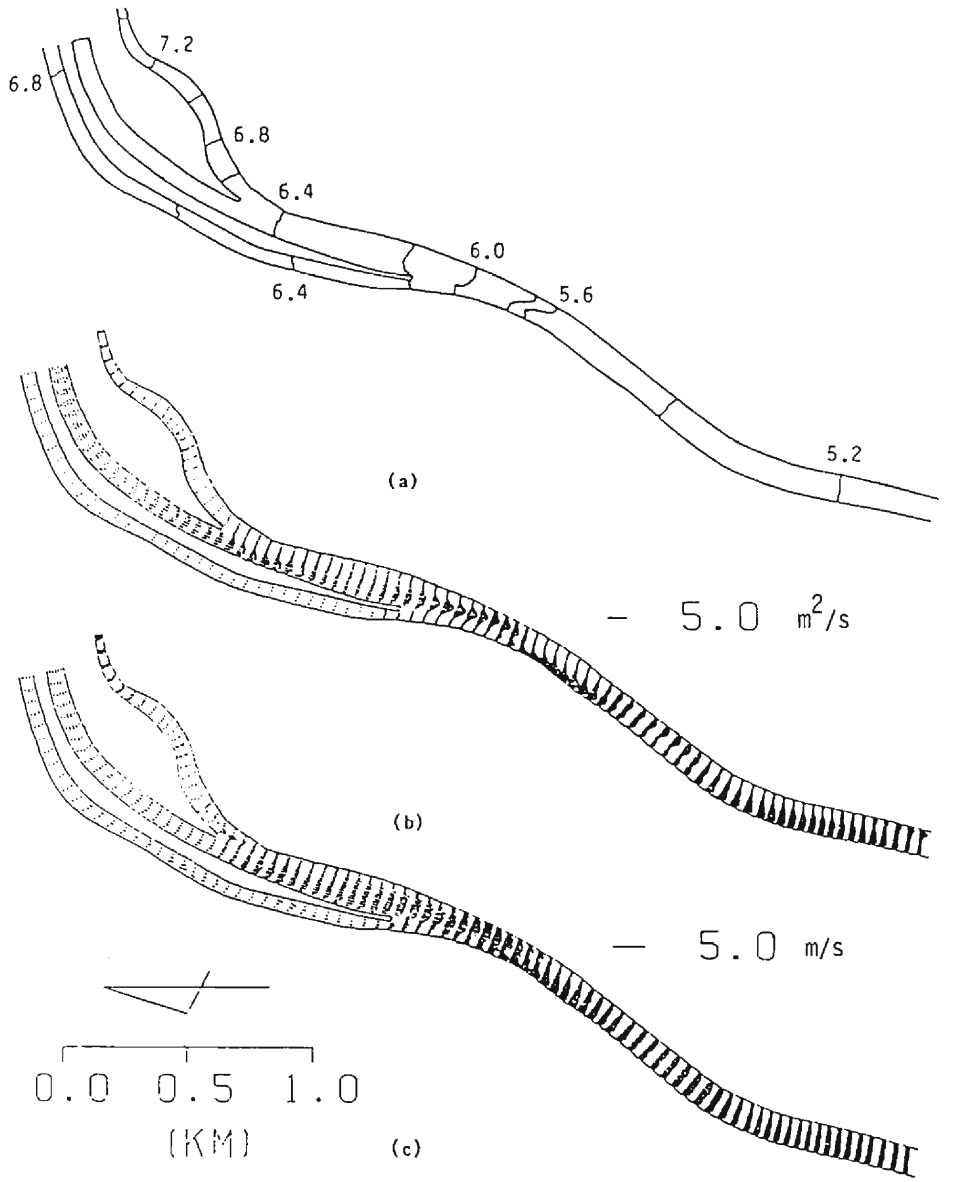

Fig. 7. Simulated results under steady state conditions in 62–0904 Test. (a) Water surface elevation contour map, (b) momentum flux vector distributions, and (c) depth-averaged velocity vector distributions.

flux vector distributions in the transverse direction are quite non-uniform, being influenced by the deep concavities. As shown in the bathymetric map of **Fig. 6(b)**, there is a concavity in the central part of the channel just below the second confluence, and the flow concentrates at the central part of the channel. In accordance with the exis-

tence of the concavity in the right bank side following the concavity upstream, the flow concentrates on the right bank side. Thus, below the second confluence, the flow changes its main route from the central part to the right bank side, to the left bank side and so on according to the variations in the river bed elevation. The depth-averaged velocity vectors change their direction in accordance with channel configuration as in the momentum flux vector distributions of **Fig. 7(b)**. However, its transverse distributions are more uniform than the momentum flux vector distributions.

The comparison of the simulated results with the observed ones was not feasible because of the lack of reliable data. However, it is felt that the simulated results gave reasonable results of flow behavior.

(2) Steady-State Concentration Distributions

The spreading of NH_3-N concentration from the Katsura River is shown in **Fig. 8(a)** according to the 62-0904 Test, and **Fig. 8(b)** for the 61-1028 Test. The high NH_3-N concentration from the Katsura River merges into the Yodo River at the lower confluence and mainly flows down along the right bank side. Its spreading width becomes longer or shorter along the flow direction, because the flow concentrates at the central part at first, next along the right bank side, then along the left bank side as described in **3. 2 (1)**. Thus, the change of the spreading width correlates with the longitudinal variation of the transverse distribution of the momentum flux vector, causing the difference of the spreading width between 62-0904 and 61-1028 Tests as will be discussed in detail in 4. 1. (2) (a).

(3) Flow Behavior and Mixing at the Confluences

The momentum flux vector distributions obtained in the simulation for the 61-1028 Test and the bathymetry at the confluence are presented in **Fig. 9(a)**, and the velocity vector distributions and the iso-depth contour map in **Fig. 9(b)**. They are close-up views of the simulation results for the entire test area, and demonstrate the flow behavior in more detail in the area including two confluences. According to the river bed elevation distribution, the flow mainly goes down along the Uji River below the upper confluence, and on the central part of the channel below the lower confluence. The water from the Kizu River merges into the water from the Uji River at the upper confluence and a part of the merged water flows toward the right bank side above the convexity between two confluences. The water from the Katsura River flows into the main stream below the lower confluence.

The variations of the flow direction are more clearly demonstrated in the velocity vector distributions in **Fig. 9(b)**. The flow toward the Uji River from other two tributaries is clearly observed in the portion of the shallow water below each of two confluences, and the divergence and convergence of flows are also clearly observed above/below the convexity located between two confluences.

Thus, the angle between the Kizu River and the Uji River at the first confluence, and that between the Katsura River and the Uji River at the second confluence are very small, with strong mixing occurring below the confluence.

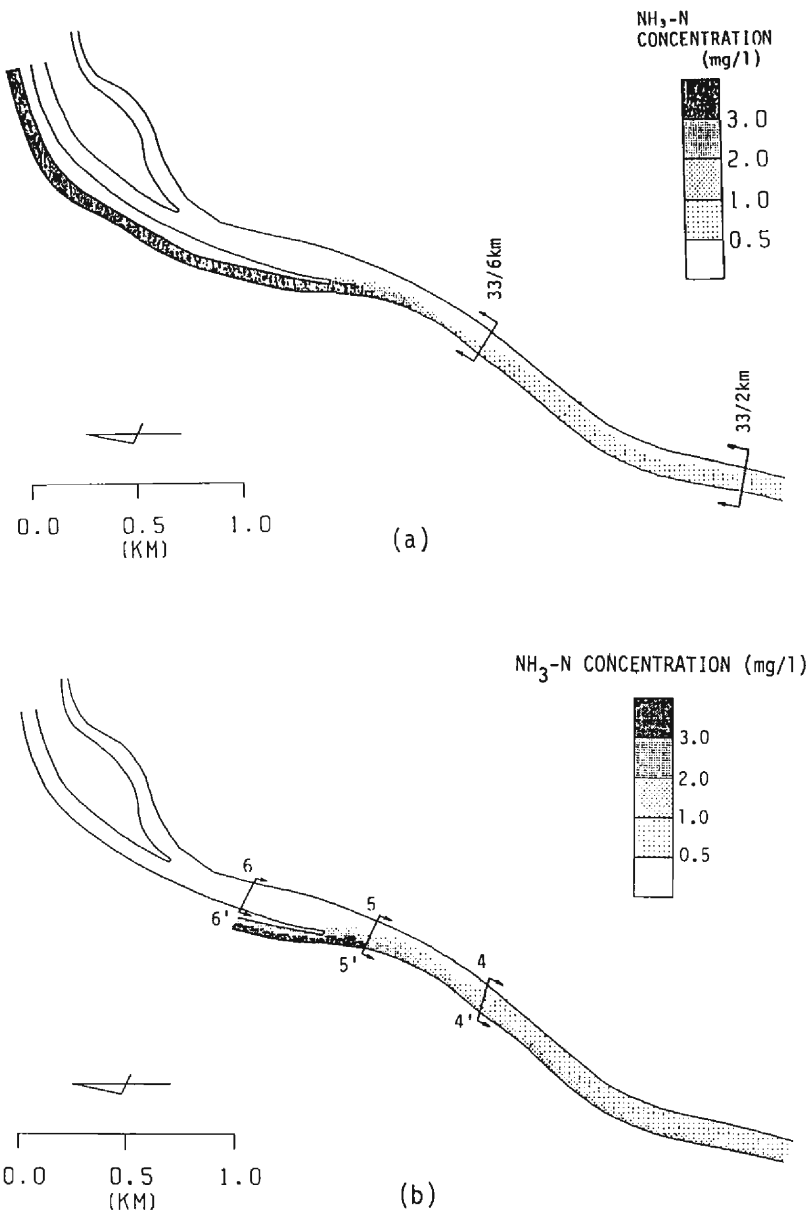

Fig. 8. Spreading of NH_3–N concentration simulated in (a) 62–0904 Test, and (b) 61–1028 Test.

The mixing at the confluences is demonstrated in **Fig. 10**, which describes the spreading of SiO_2 concentration according to the 61–1028 Test. The high SiO_2 concentration water from the Kizu River spreads widely just below the upstream confluence, being transported by the flow toward the Uji River, and it disperses throughout the channel

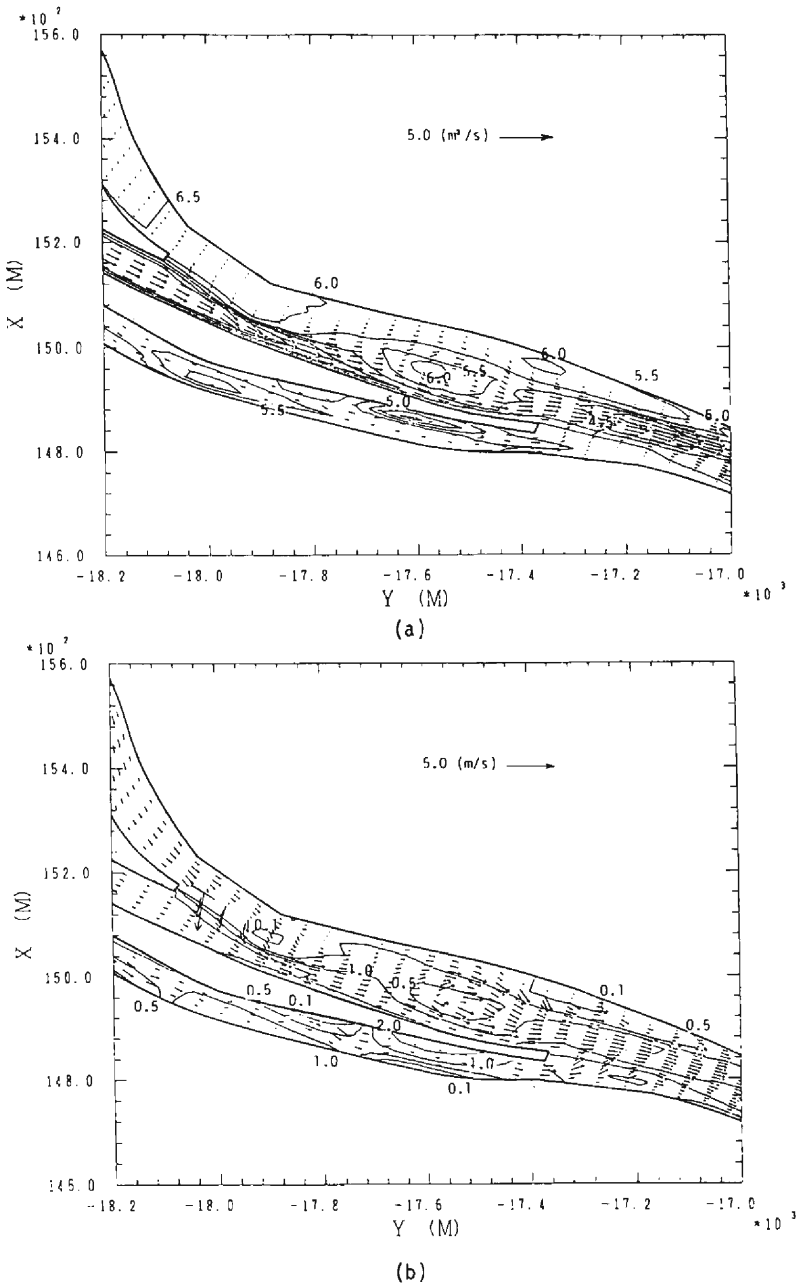

Fig. 9. Flow behavior and mixing at the confluence simulated in 61–1028 Test. (a) Momentum flux vector distributions and the iso-contour map of the bottom elevation, and (b) depth-averaged velocity vector distributions and the iso-contour lines of water depth.

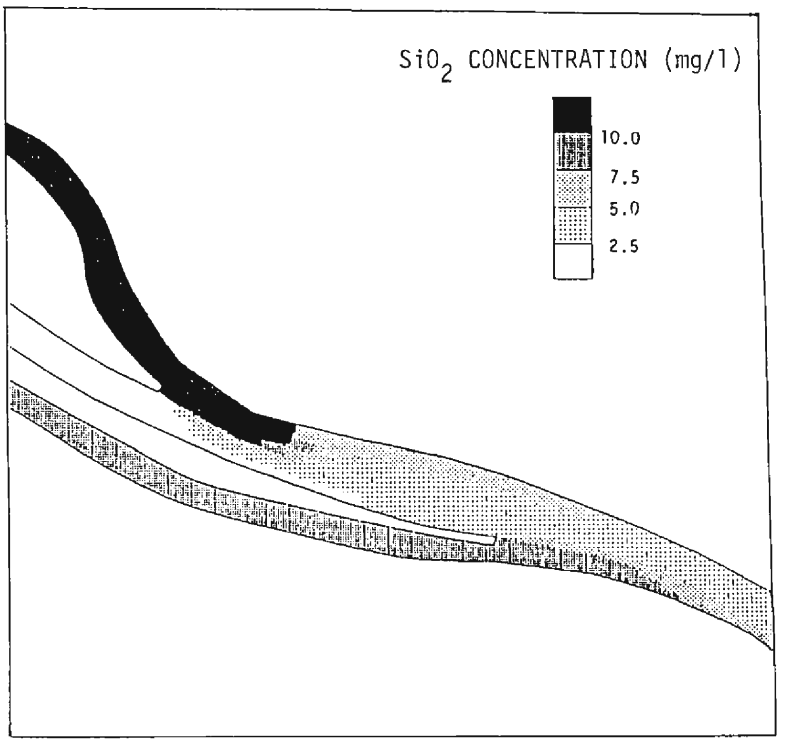

Fig. 10. Spreading of SiO_2 concentration at the confluences simulated in 61-1028 Test.

above the convexity by the flow diverged. The SiO_2 concentration from the Katsura River also spreads into the Uji River below the lower confluence, being transported by the flow into the Uji River, but it is not as evident as that below the upper confluence.

(4) Transverse Distributions of Concentration

The transverse distributions of NH_3-N concentration at the sections of 33.6km and 36.1km obtained in the simulation for 62-0904 Test under various transverse dispersion coefficients are comparatively presented with the measured ones in **Fig. 11(a)** and **(b)**. The influence of the magnitude of the transverse dispersion coefficient on the transverse concentration distribution is small at both sections of 33.6km and 32.2km, so that the larger transverse dispersion coefficient causes a small decrease in NH_3-N concentration near the right bank side. Simulated results under the non-dimensional dispersion coefficient $\alpha_T = D_T/hu_* = 0.20$ and 2.00 have nearly the same concentration distribution and agree well with the observed ones as shown in **Fig. 11(a)**. Therefore, it is concluded that the magnitude of the transverse dispersion coefficient at the confluence is of the same order as those measured in other straight laboratory flumes and/or river channels[15]. It is also suggested that convective transport plays a more important role in the transverse mixing in the Yodo River Confluence than the gradient tyme mass transport because the

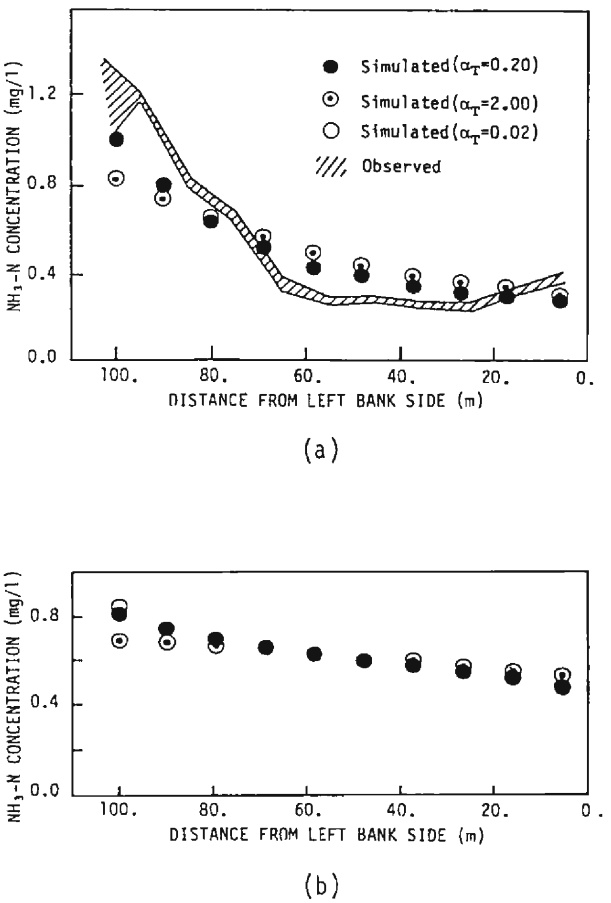

Fig. 11. Transverse distributions of NH_3–N concentration simulated in 62–0904 Test and measured ones for (a) 33.6km section, and for (b) 32.2km section. Circles denote simulated values under various dispersion coefficients, and the hatched area shows the observed concentration distribution.

transverse distribution of the momentum flux vector is quite non-uniform and the mixing is mainly governed by convection as decribed above.

The transverse distributions of NH_3–N concentration obtained in the simulation for 61–1028 Test are comparatively presented with field-measured distributions in **Fig. 12(a)**, **(b)**, and **(c)**. NH_3–N concentrations from the Uji and Kizu River mix well and the resulting distribution is almost uniform at 6–6′ (34.8km) section which is 400. m below the first confluence of the two tributaries, as shown in **Fig. 12(a)**. This is caused by the strong merging of the Kizu River into the Uji River and the divergence of merged water above the convexity as stated earlier in **3. 2 (3)**. Simulated results agree well with the observed concentration distribution.

Observed and simulated NH_3–N concentration distributions at 5–5′ (34.2km) section are presented in **Fig. 12(b)**. The test section is located at 200. m below the confluence

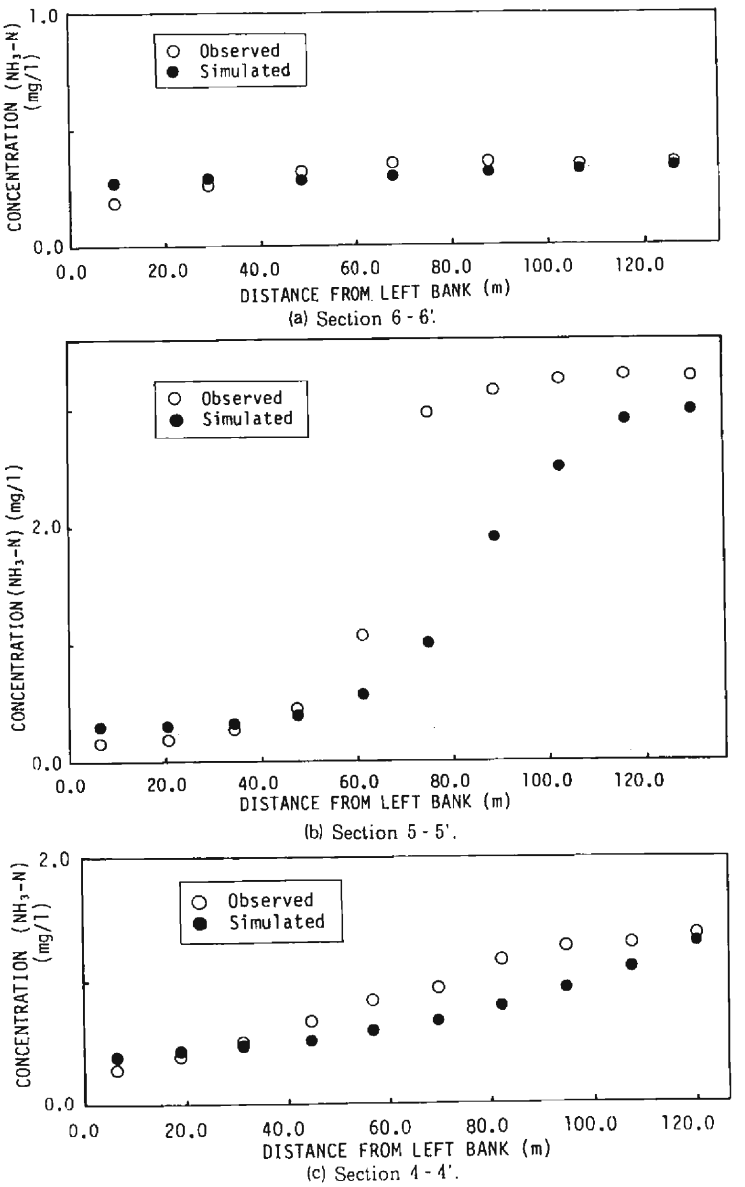

Fig. 12. Transverse distributions of NH_3–N concentration simulated in 61–1028 Test and measured ones. (a) 6–6′ (34.8km) section, (b) 5–5′ (34.2km) section, and (c) 4–4′ (33.6km) section.

of the Uji River and the Katsura River, which contains high NH_3–N concentration. The river is wide below the confluence and the distance between the confluence and the test section is not long, so that mixing of the water from the two rivers is not strong; a part of the water from the Katsura River flows down along the right bank side below the

confluence and NH_3–N concentration near the right bank side is still high, and that near the left–bank side is still low.

At the section 4–4′ (33.6km), the concentration distribution is more uniform, that is, the concentration near the right bank side becomes much lower, while increasing a little higher near the left bank side as shown in **Fig. 12(c)**, because the flow concentrates at the central part of the channel at the 5–5′ section, but at the right–bank side at the 4–4′ section as described in **3. 2 (1)**. This change of the flow rate distribution causes the strong mixing of water, that is, the low NH_3–N concentration water at the central part of the channel dilutes the high concentration water near the right bank side. The dispersion transport makes the concentration near the left bank side a little higher. The agreement between observed and simulated concentration distributions at both 5–5′ and 4–4′ sections are reasonable, with some small difference between them observed near the central mart of the channel.

The simulated results of SiO_2 concentration for 61–1028 Test are also comparatively illustrated with field–measurement concentration distributions at 6–6′, 5–5′ and 4–4′ sections in **Figs. 13(a)**, **(b)** and **(c)**. Simulated results at the 6–6′ section do not agree well with the observed ones, but those at the 5–5′ and 4–4′ sections are much better. A special feature observed through these three comparisons is the difference between the measured and simulated concentrations near the left bank side, with the results at the 5–5′ and 4–4′ section being in very good agreement with each other except for this portion. This difference is thought to be caused by insufficient upstream boundary condition measured in the Kizu River, the entrainment from the bottom, and/or effluent of SiO_2 from small tributaries which is not included in the numerical models between the upstream boundary and the 6–6′ section, because the concentration measured near the left bank side at the lower two sections was higher than that at the upstream cross–section.

Thus, the results for NH_3–N agreed well with the observed ones except in the center of the river, and those for SiO_2 also showed fine agreement with each other except near the left bank side. It is thus concluded that the numerical models are applicable for analyzing transverse mixing at rivers with complicated geometry. The discrepancies between measured and observed values for NH_3–N and SiO_2 concentrations suggest the need for more detailed field measurement and/or higher modeling.

Two sets of simulation tests for verifying the mathematical models described in **Section 2** were carried out in the Yodo River System which includes the confluences of three tributaries. The simulated flow behavior was not compared with field data; however, the water surface elevation contour lines, the momentum flux vector distributions, and the velocity vector distributions obtained in the simulation are reasonable ones, and their features are discussed in detail with relation to the bathymetry of the study area. The simulated concentration distributions were successfully compared with the distributions obtained in 62–0904 and 61–1028 field measurements. The mechanism of mixing in the Yodo River Confluence are discussed in detail with relation to flow behavior. The estimated transverse mixing coefficient being less than $2.0hu_*$, it is suggested that convective transport plays a more important role than dispersive transport.

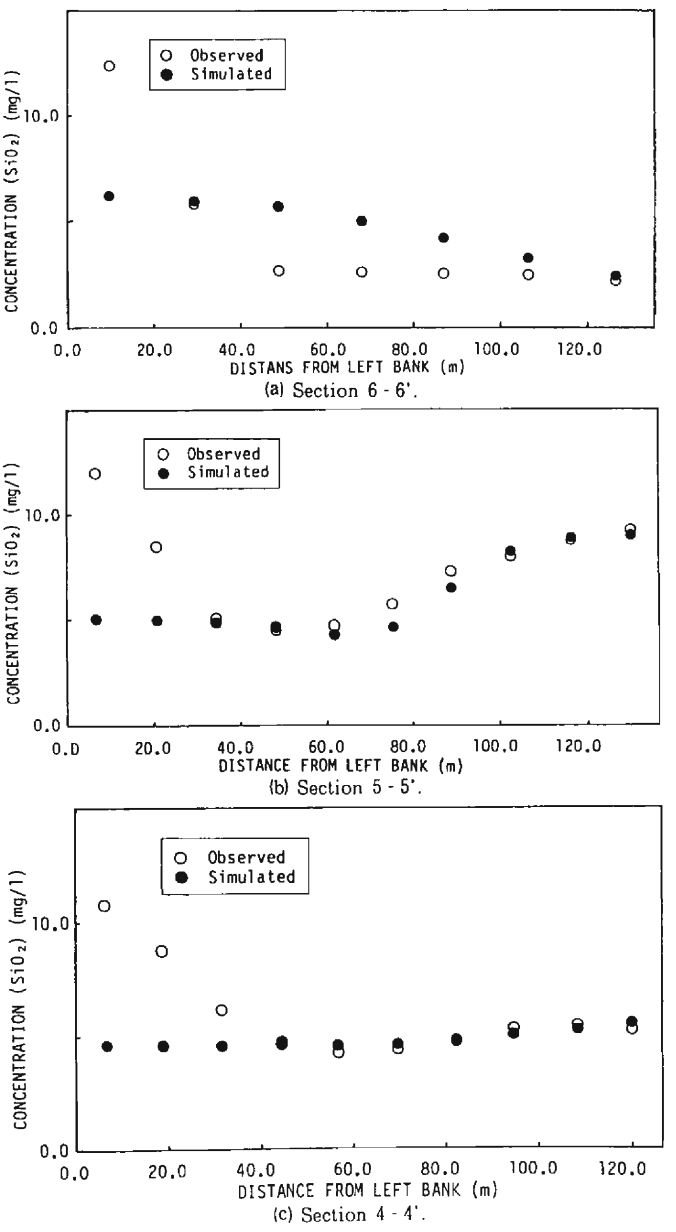

Fig. 13. Transverse distributions of SiO_2 concentration simulated in 61-1028 Test and measured ones. (a) 6-6′ (34.8km) section, (b) 5-5′ (34.2km) section, and (c) 4-4′ (33.6km) section.

4 Mechanism of Transverse Mixing in the Yodo River System

As described in **1. 2**, investigation of the mechanism of the mixing at/below the confluence of the Yodo River System is urgently required in terms of environmental conservation, as well as the very interesting questions of the mixing at the confluence in open-channel hydraulics. This section will study the mixing at/below the confluence of the Yodo River System under various hydraulic conditions and investigate the mechanism of mixing in terms of the aspects stated above by the numerical and the simplified hydraulic experiments.

The hydraulic conditions influencing the mixing at/below the confluence can be expected to be: (1) the magnitude of the transverse dispersion/mixing coefficient, (2) flow regimes of river system and flow rate of each of tributaries to the total discharge below the confluence, (3) distributions of the river bed elevation at/below the confluence, (4) geometrical features of the confluence such as the angle between each of tributaries and the main stream, and (5) the water surface elevation at the lower boundary. Therefore, the first series of the numerical experiments for the mixing in the Yodo River System will be described in **4. 1** under the various flow regimes listed in **Table 1** in **Section 1.** It covers the flow regimes between the annual average discharge and the drought discharge during which the water quality pollution problem is the most serious. In **4. 2**, the second series will also be done under the same boundary conditions of the first series, but with two sets of hypothetical cross-section channels: (a) the rectangular cross-section channel, and (b) the river-channel dredged along the right bank side, while the alignment of both model rivers is similar to the actual river. The influence of the magnitude of transverse mixing coefficient will also be examined through these two sets of numerical experiments. The other possible influence of conditions (4) and (5) has already been reported in the writers' previous papers[16),17)]. Additionally, the simplified hydraulic model experiment for the dispersion in the downstream part from the Yodo River Confluence will be described in **4. 3** to confirm the results obtained in the numerical experiments.

4. 1 Numerical Experiments in an Actual River System

The numerical simulation models and their procedures are similar to those described in **Section 3**, therefore they are not reviewed, but only the conditions and results of the numerical experiments under various hydraulic conditions will be described in the following sub-sections.

(1) Conditions of Numerical Experiments

The numerical experiments were conducted under the four different hydraulic conditions listed in **Table 1**. The discharge of each tributary is from "Annual Report for 1980: Discharge Measurements in Important Rivers in Japan" (River Bureau, Ministry of Construction, 1982), and the water surface elevation at the downstream boundary is calculated by use of those measured at Takahama stage-observatory and listed in "Annual Report for 1980: Stage Measurements in Important Rivers in Kinki Region, Japan" (Kinki Regional Bureau, Ministry of Construction, 1982). The concentration at the

upstream boundary of each tributary is hypothetical, and two sets of conditions are given, that is, $C=100\%$ at the Katsura River and $C=0$ at the Uji River and the Kizu River for the first set, and $C=100\%$ at the Kizu River and $C=0$ at the Katsura River and the Kizu River for the second set.

The each value of tubulent viscosity, roughness coefficient and the longitudinal mixing coefficient is the same as those in **Section 3.** The transverse dispersion coefficient has been measured in laboratory by many investigators[11),12),13),14)], and in rivers by Yotsukura et al[18)]. They are summarized in Yotsukura and Nakamura[19)], and texts[15),20)]; its magnitude is of the order of $0.1\sim0.2hu_*$ in laboratory, and $0.4\sim0.8hu_*$ in straight rivers. The magnitude of the transverse dispersion/mixing coefficient estimated in the Yodo River was reported at $D_T=0.05\text{m}^2/\text{s}$ by Nambu[21)], $D_T/hu_*=0.6\sim2.0$ by Li, Yagi and Sueishi[4)], $D_T/hu_*=2.2$ by Yoneda, Iwata and Inoue[22)], and so on. The magnitude of the transverse dispersion coefficient described above is larger than those summarized in **3.1,** but the smaller dispersion coefficient $0.2hu_*$ is commonly applied to this numerical experiment, and a different order of magnitude of coefficient is also examined.

(2) Results and Discussion

(a) Effects of flow Regime

Flow fields: The water surface elevation contour maps, the momentum flux vector distributions and the depth-averaged velocity vector distributions are shown in **Figs. 14, 15,** and **16,** respectively. Each figure illustrates those obtained under four different flow regimes. The features of flow fields obtained under each hydraulic condition are quite similar to each other and to those described in the verification tests in **Section 3.** The distinguishable features among the four flow regimes are observed in the distributions of the momentum flux vector and the depth-averaged velocity, and they are summarized as:

1. The river flow is mainly in the lower part of the river bed elevation in the channel, and the water route in the channel is thus developed in accordance with the river bed topography, that is, concavities and convexities as illustrated in the topographical map of **Fig. 6(b)**.
2. The momentum flux vector distributions are non-uniform in the transverse direction, and its transverse distributions are also varied in the longitudinal direction.
3. These distributions are influenced by flow regimes; that is, the non-uniformity of the momentum flux vector distributions becomes larger as the discharge becomes smaller.
4. The distributions of the depth-averaged velocity vector are also affected by the river bed topography and the flow regimes.
5. The influence of the flow regime on the velocity vector distributions is clearly observed in the confluences, where the water-depth is shallow and the river bed topography is less uniform, and the direction of the depth-averaged velocity vector is changed in the confluences.
6. However, it is smaller below the second confluence, because the river bed slope is very mild and the water surface profile is backwater below the confluence.

These features are more clearly observed in the close illustrations of **Fig. 17** in which

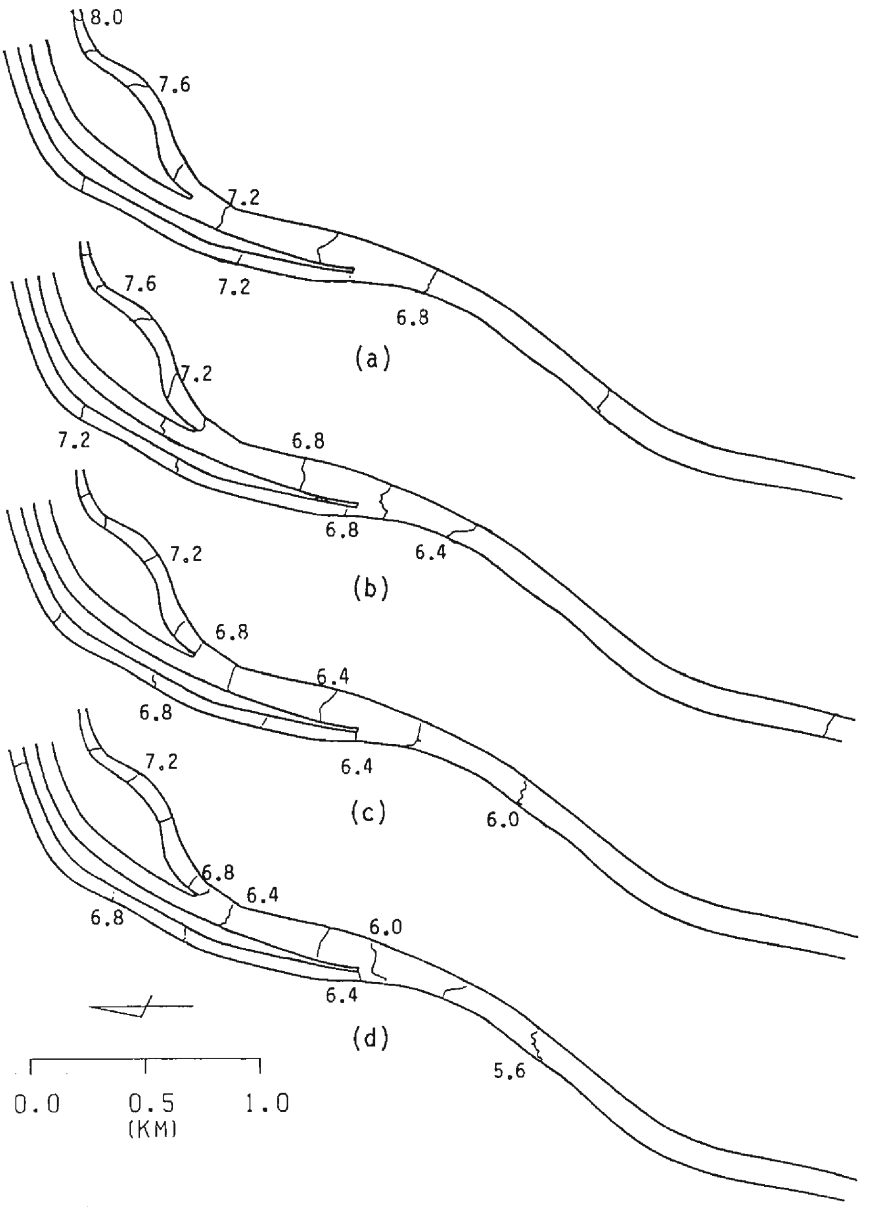

Fig. 14. Water surface elevation contour maps in the Yodo River System under various flow regimes. (a) Annual average discharge, (b) ordinary (185-day) water discharge, (c) low water (275-day) discharge, and (d) drought (355-day) discharge.

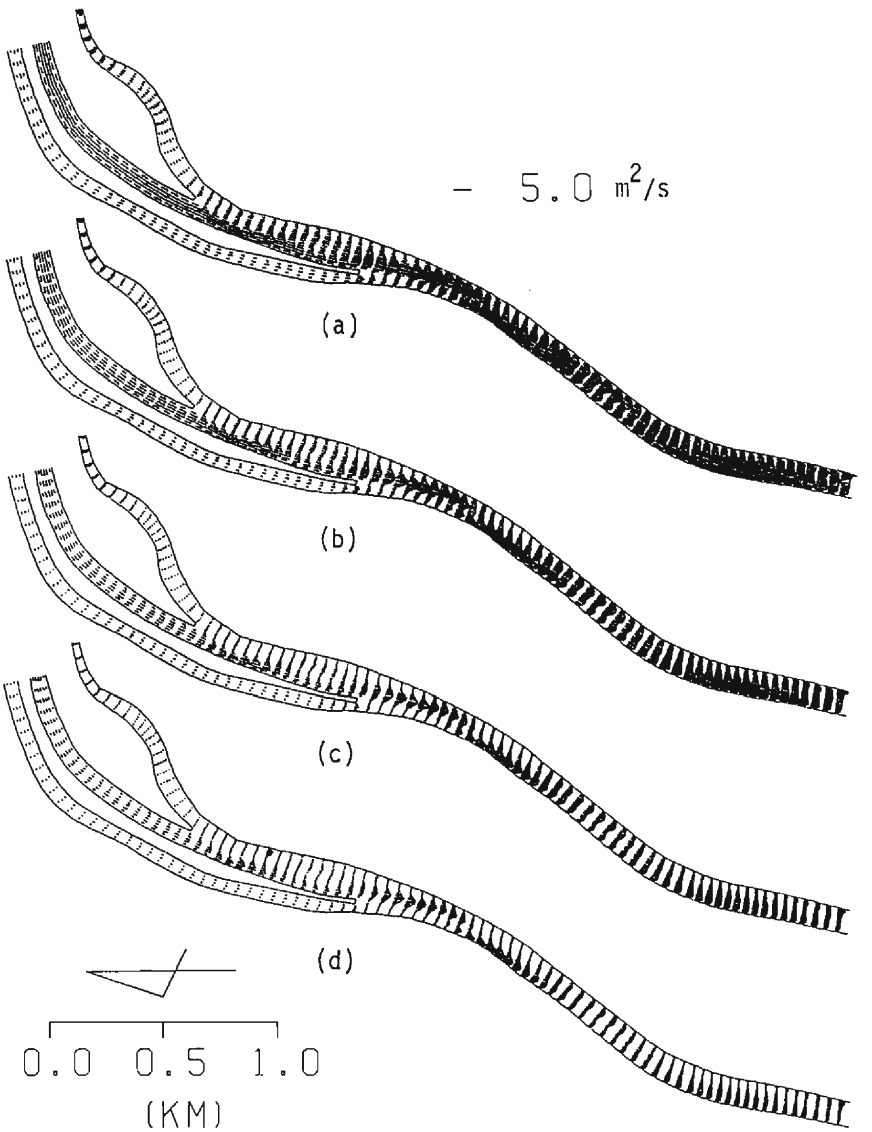

Fig. 15. Momentum flux vector distributions in the Yodo River System simulated under various flow regimes. (a) Annual average discharge, (b) ordinary (185-day) water discharge, (c) low water (275-day) discharge, and (d) drought (355-day) discharge.

the momentum flux vector and the depth-averaged velocity vector distributions are illustrated between two confluences under regimes of (a) annual average discharge, and (b) drought discharge.

Concentration distributions: The steady state concentration distributions of tracer cloud

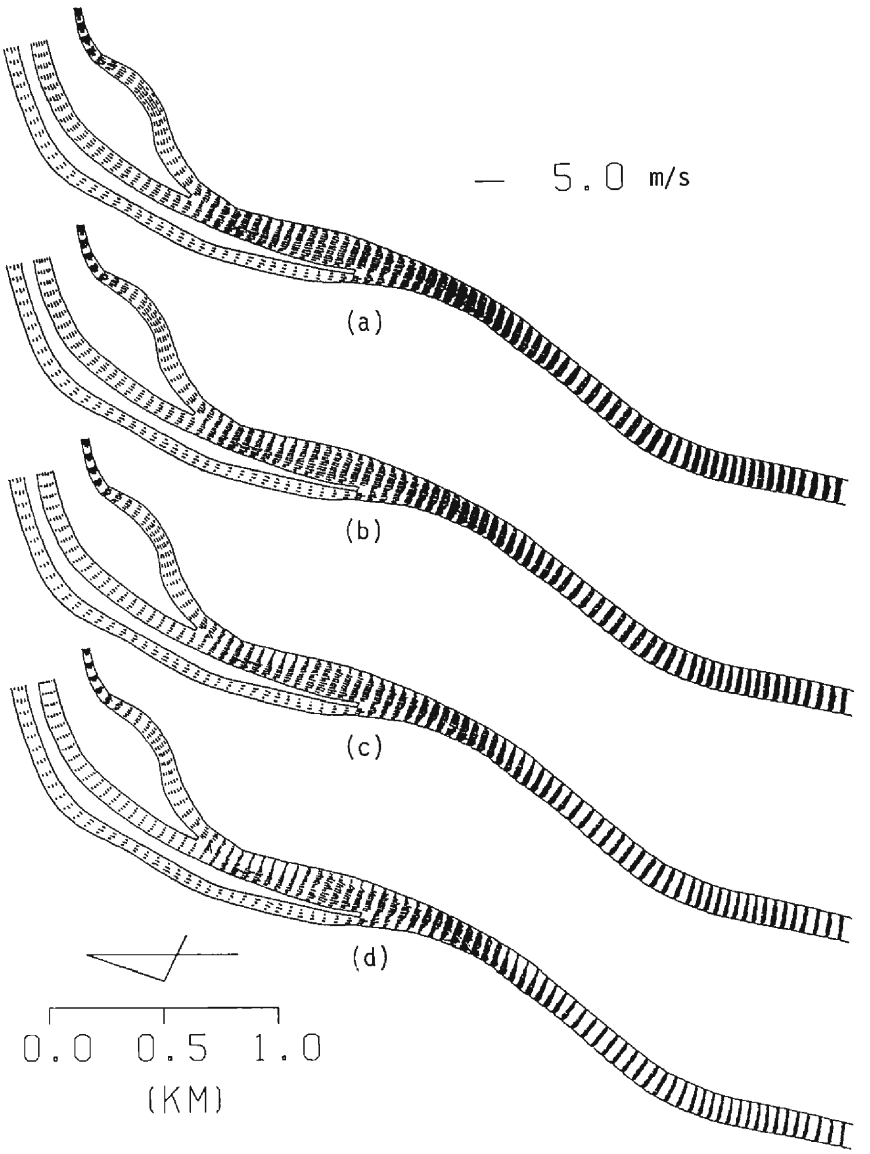

Fig. 16. Depth–averaged velocity vector distributions in the Yodo River System simulated under various flow regimes. (a) Annual average discharge, (b) ordinary (185–day) water discharge, (c) low water (275–day) discharge, and (d) drought (355–day) discharge.

from the Katsura River under the four flow regimes are shown in **Fig. 18**(**a**), (**b**), (**c**) and (**d**). The tracer cloud from the Katsura River merges into the main channel at the second confluence, and mainly flows down along the right bank side. It disperses in the transverse direction, but the spreading width changes in the longitudinal direction, that is,

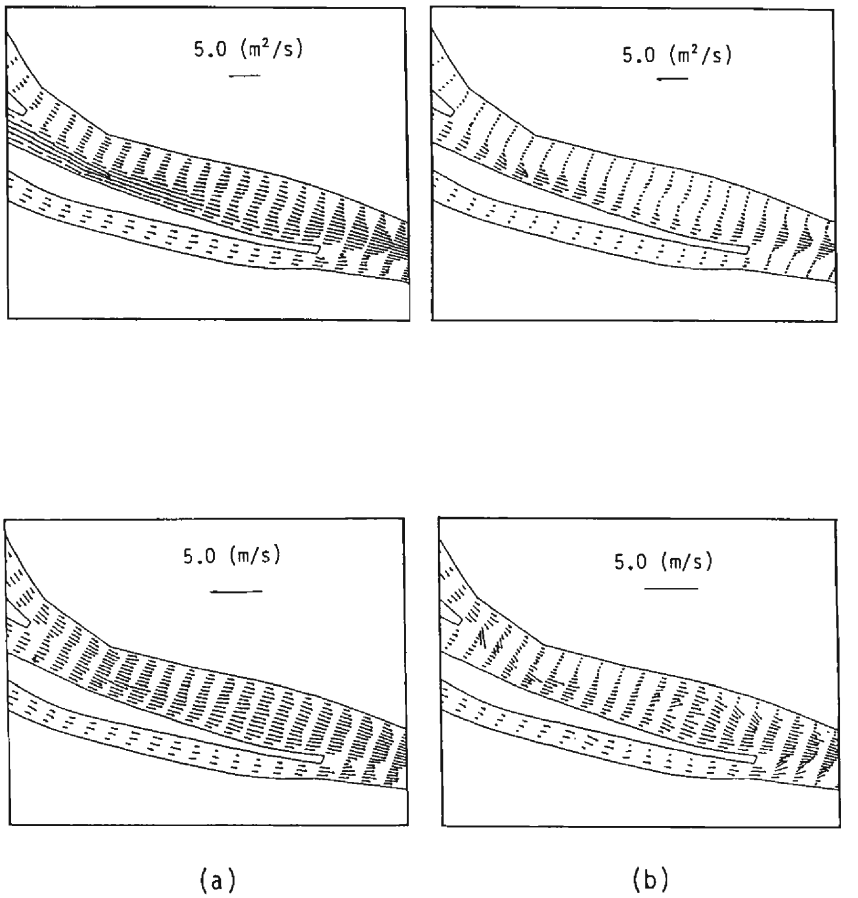

Fig. 17. Distributions of the momentum flux vector (upper figures) and the depth-averaged velocity vector (lower figures) at the confluences of the Yodo River System. (a) Annual average discharge, and (b) drought (355-day) discharge.

it becomes longer and/or shorter while flowing as decribed in **3. 2** (**4**). The distinguishable feature among the four regimes is that the spreading width of tracer cloud grows wider and wider with the decrease of discharge, that is, the transverse concentration distributions are less uniform in the regime of annual average discharge, and more uniform in the regime of drought discharge. This feature is more clearly demonstrated in **Fig. 19**, which illustrates the transverse distributions of concentration at the 33.6km section under the four flow regimes for (a) the tracer from the Katsura River, and for (b) the tracer from the Kizu River. The notable characteristics of the transverse mixing are as follows :

1. The momentum flux vector distributions are more uniform in the regime of annual average discharge, and less uniform in the regime of drought discharge in both longitudinal and transverse directions.

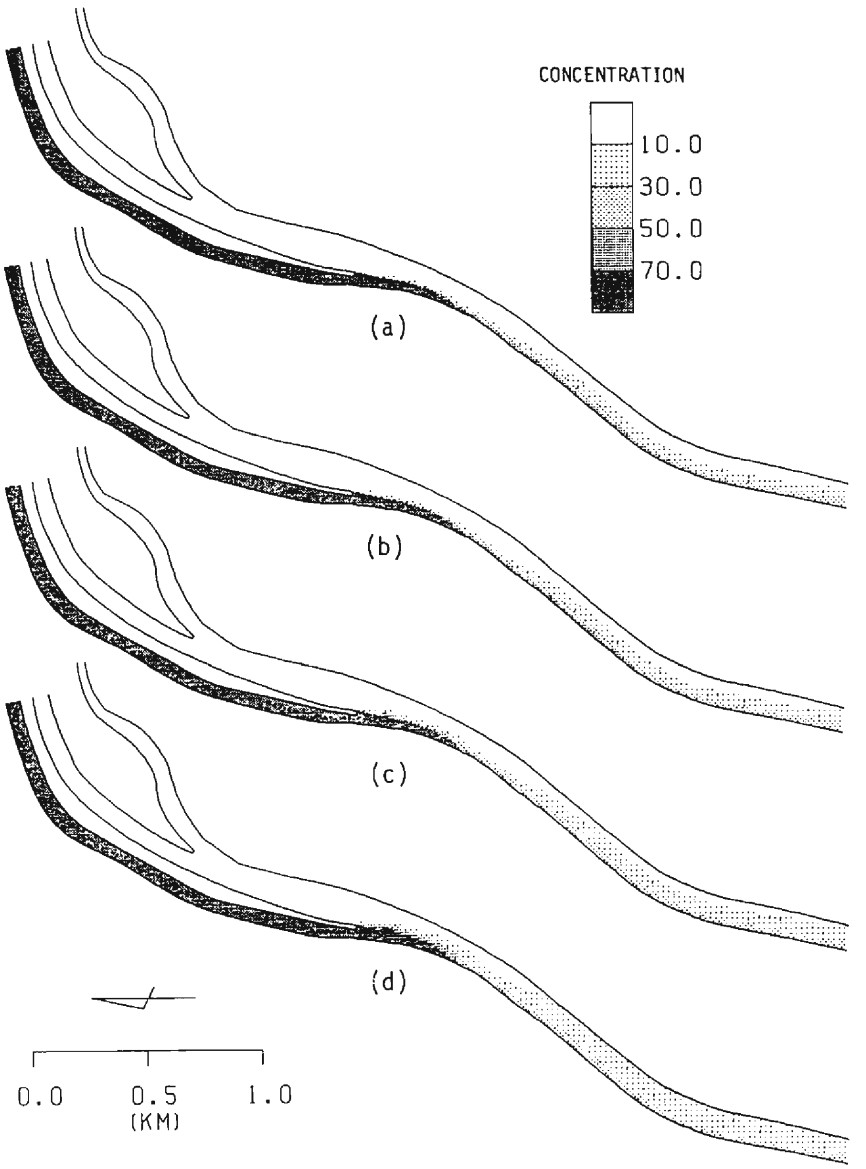

Fig. 18. Distributions of concentration from the Katsura River in the Yodo River System simulated under various flow regimes. (a) Annual average discharge, (b) ordinary (185-day) water discharge, (c) low water (275-day) discharge, and (d) drought (355-day) discharge.

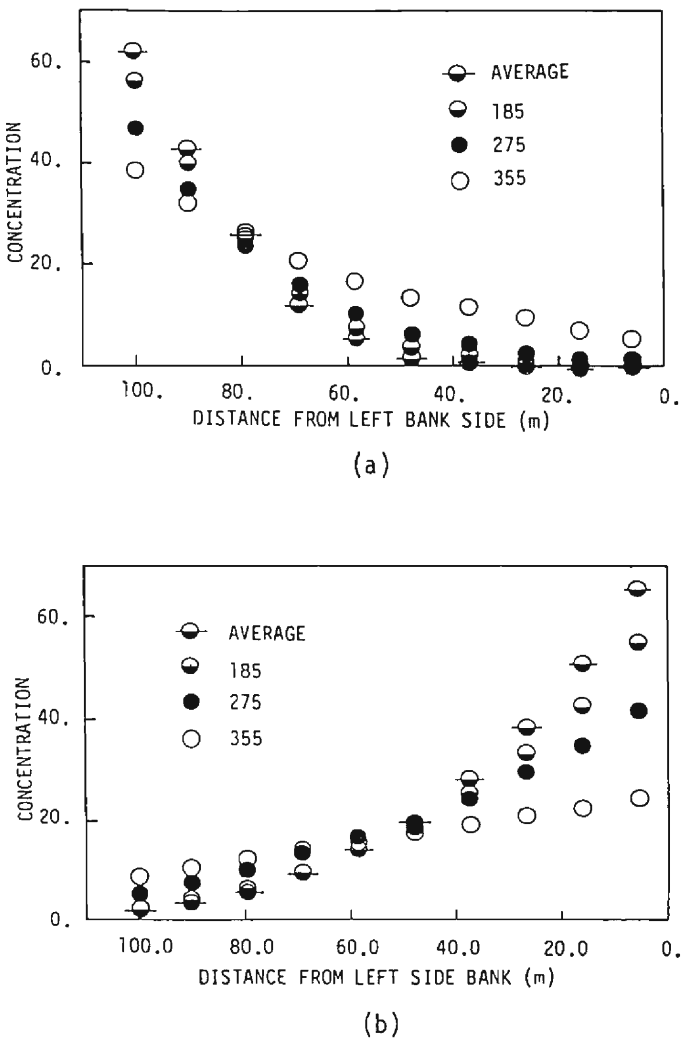

Fig. 19. Transverse distributions of concentration at 33.6km section simulated under the various flow regimes. (a) Tracer from the Katsura River, and (b) tracer from the Kizu River.

2. These variations of the momentum flux vector distribution cause the transverse mixing of tracer cloud by convective transport as well as the transverse dispersion.
3. The longitudinal variation of the transverse distributions of the momentum flux vector is stronger with decrease of discharge as described above, whereby, the transverse mixing accelerates.
4. Thus, as the discharge becomes smaller, the mixing of the tracer cloud in the transverse direction accelerates by convective transport, whereby, the transverse distribution of the tracer becomes more uniform.

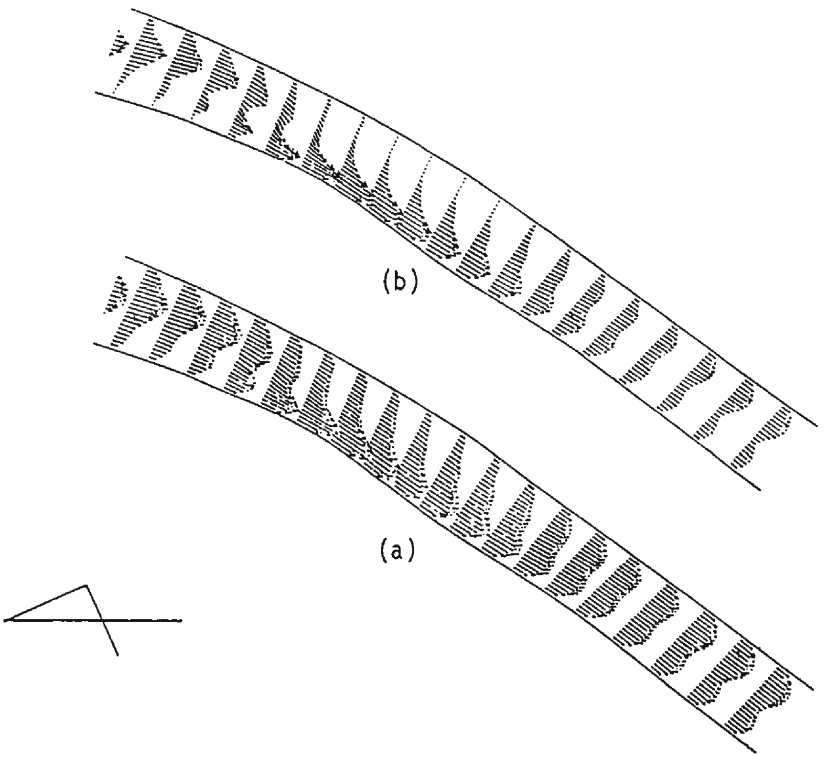

Fig. 20. Patterns of momentum flux vector distributions near the reach from 33.0km to 34.0km sections in the Yodo River System simulated in (a) annual average discharge, and (b) drought (355-day) discharge.

Figs. 20(**a**) and (**b**) show close views of the momentum flux distributions between 34.0 and 33.0km sections below the confluences, and **Figs. 21**(**a**) and (**b**) the corresponding concentration distributions of the tracer cloud from the Katsura River. These figures more definitely demonstrate the mechanism of the transverse mixing downstream from the Yodo River Confluence.

(b) Effect of Transverse Mixing Coefficient

The influence of the transverse mixing cofficient was examined under the regime of ordinary water (185-day) discharge because it has already been examined in **Section 3** under 62-0904 Test for verification, in which the discharge was between low water (275-day) and drought (355-day) discharges. The magnitude of the transverse mixing coefficient is specified at $\alpha_T = D_T/hu_* = 0.02$, 0.2, or 2.00. The transverse distributions of tracer concentration from the Katsura River are presented in **Figs. 22** for (a) 33.6km section, and (b) 32.08km section. The variation among the three concentration distribution curves is not so large, but the concentration distribution is more uniform as a larger transverse mixing coefficient is specified. Comparing the results in **Fig. 11** for the 62-0904 Test, it is disclosed to be more effective with increase of the discharge. However,

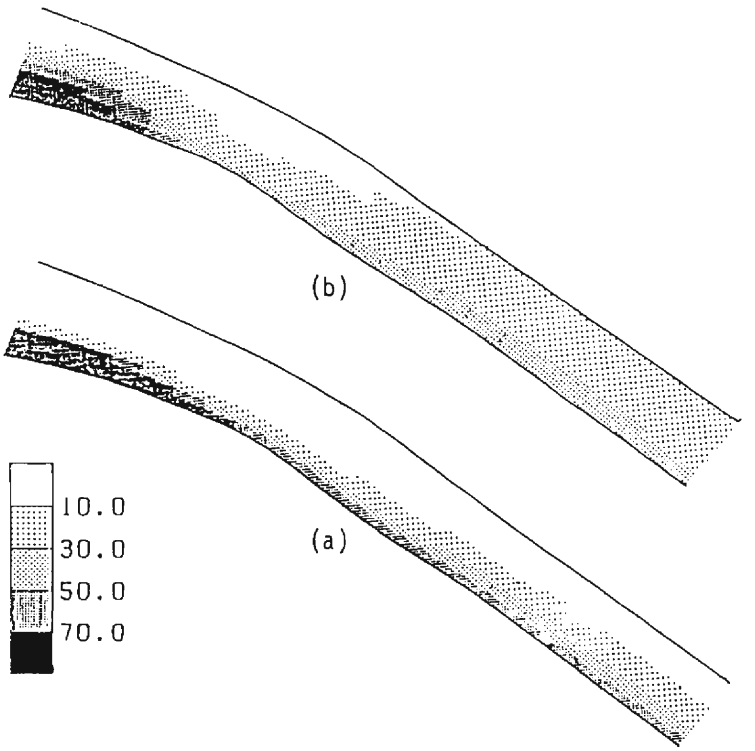

Fig. 21. Patterns of distributions of concentration from the Katsura River near the reach from 33.0km and 34.0km sections in the Yodo River System simulated in (a) annual average discharge, and (b) drought (355-day) discharge.

different flow regimes cause much more varied concentration distributions as shown in **Fig. 19**, and the magnitude of the transverse mixing coefficient has less effect on the transverse concentration distributions.

Thus, it was disclosed that transverse mixing consists of the gradient type mass transport as well as the convective transport caused by the change of water-route in the channel, with the latter factor being more dominant in the Yodo River System which has non-uniform distribution of river bed elevation in both the longitudinal and the transverse directions.

4. 2 Numerical Experiments in a River System of Various Cross-Section Channels

(1) Outlines of Experiments

The first set of the numerical experiments in **4. 1** disclosed that the non-uniform distributions of the river bed elevation is more effective with the transverse mixing in the Yodo River System, and this sub-section will investigate the mixing in two kinds of model channels of the Yodo River System, that is, Model river (a) with rectangular cross-section, and Model river (b) in which the river channel is dredged along the right bank-

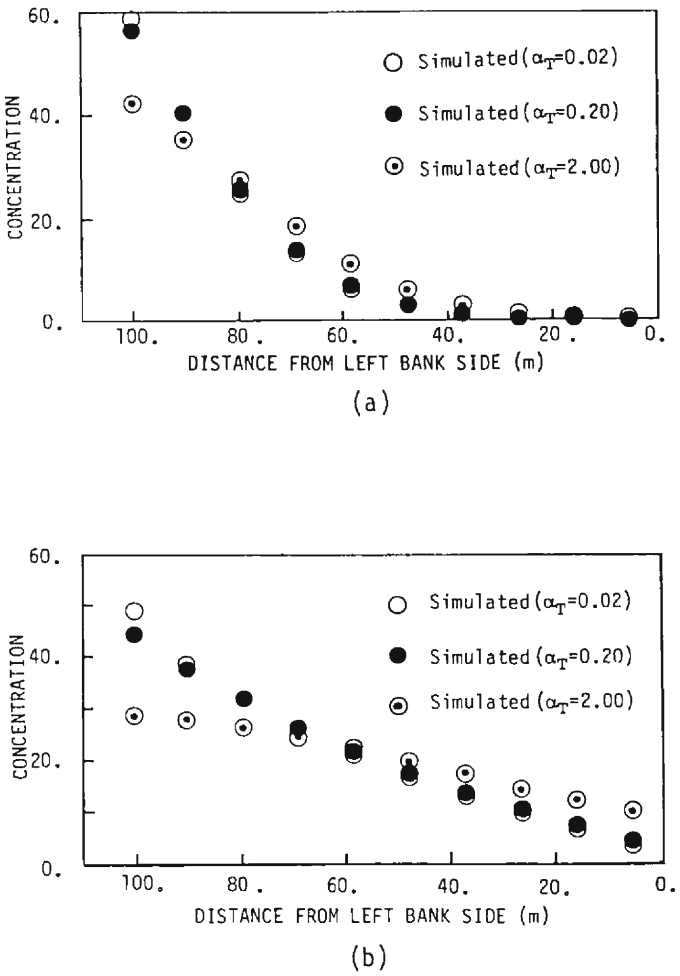

Fig. 22. Transverse distributions of tracer concentration from the Katsura River under various transverse mixing coefficients in ordinary (185-day) discharge condition for (a) 33.6km section, and (b) 32.08km section.

side. The bathymetry of the two model rivers are illustrated in **Fig. 23** for Model river (a), and Model river (b). These channel geometries are hypothetical ones, but were actually encountered during/after river improvement works. The simulation conditions are similar to those in 62-0904 Test in **Section 3** and to the first set of numerical experiments in **4. 1.**

(2) Results and Discussions on Experiments under Various Cross-Section Channels

(a) Flow Fields

The momentum flux vector distributions are presented in **Fig. 24** for Model river (a), and Model river (b). Comparing the results in the actual river channel presented in

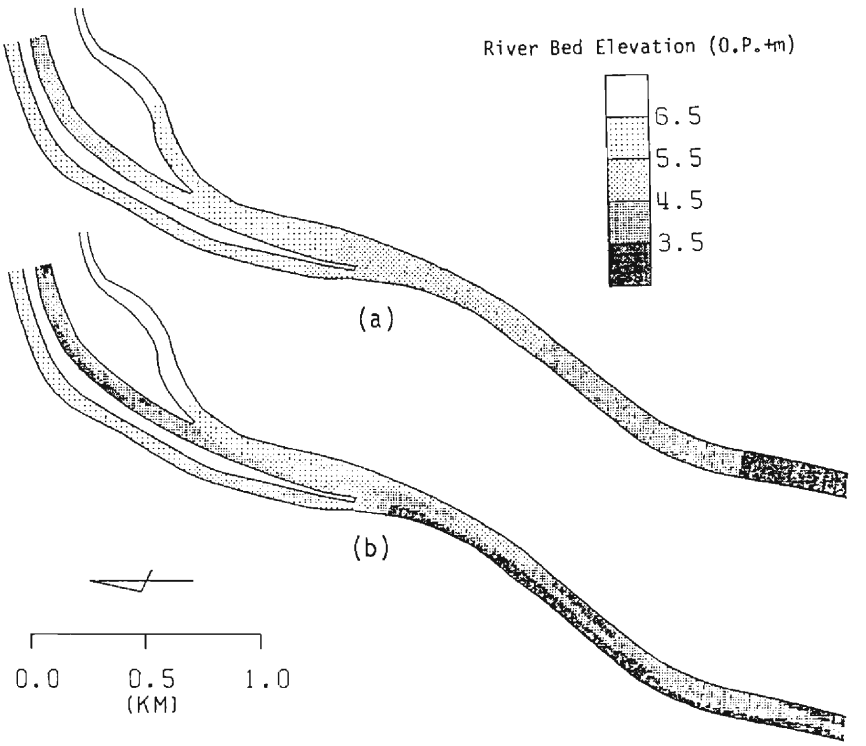

Fig. 23. Bathymetric maps of model rivers for Model river (a), and Model river (b).

Fig. 7 in **Section 3**, the momentum flux vector distributions in the lateral direction are quite uniform in Model river (a), and its longitudinal variations are very small. On the contrary, the momentum flux vector distributions in Model river (b) is quite non-uniform in the transverse direction, but uniform in the longitudinal direction. The flows from three tributaries converge and concentrate on the right side of the channel and flow down along the right bank side. Thus, the channel geometry is quite influential on the flow fields.

(b) Concentration Distributions

Spreading of the tracer from the Katsura River is also illustrated in **Figs. 25**(**a**) and (**b**). By comparison with the concentration distributions obtained in the actual river channel presented in **Fig. 8** in **Section 3**, the spreading width of tracer is limited and much smaller than actuality. The transverse concentration distributions at 33.6km section section under three different channel conditions for 62-0904 Test are comparatively presented in **Fig. 26.** The concentration distribution is quite non-uniform in Model river (a), and the mixing is controlled because the momentum flux vector distributions are uniform in the longitudinal direction, and so the convective transport in the transverse direction is very small and the mixing is mainly caused by the transverse dispersion. The spreading width is also limited in Model river (b), but its peak concentration is small as that in the

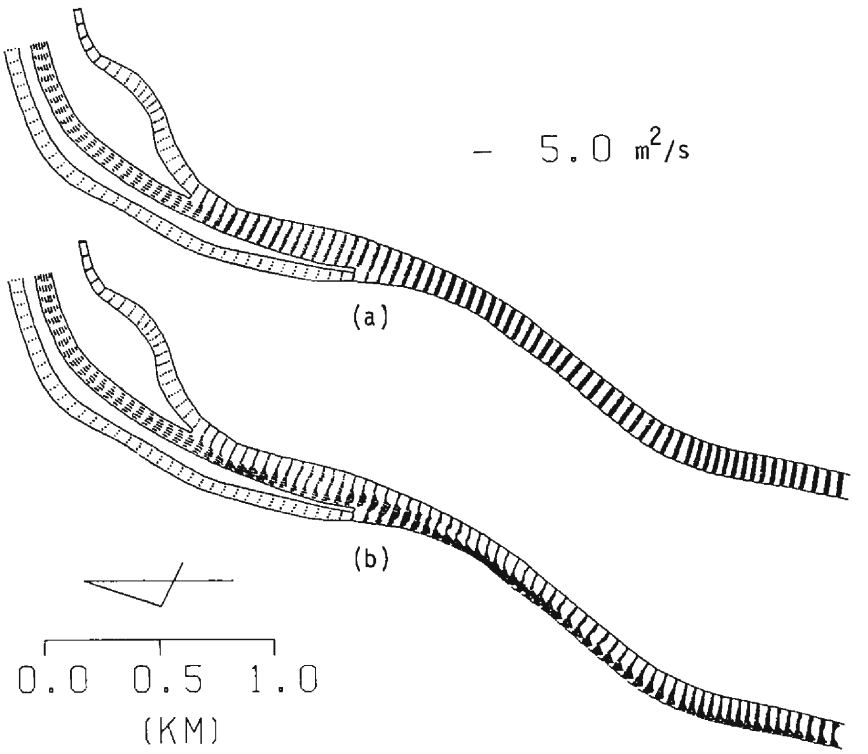

Fig. 24. Momentum flux vector distributions under Regime 62–0904 in model rivers for Model river (a), and Model river (b).

actual river, because the flows from three tributaries strongly merge together below the confluence, therefore the high concentration from the Katsura River was diluted by the waters from the Uji and the Kizu Rivers. Below the confluence, the momentum flux vector distributions are non-uniform in the transverse direction, but uniform in the longitudinal direction, and the spreading width is limited. Thus, the channel geometry has quite an effect on the spreading of the concentration, because the flow fields are affected by the channel geometry.

(3) Results and Discussions on Experiments in Rectangular Cross-Section Channels under Various Flow Regimes

(a) Flow Fields

The water surface elevation contour maps, the momentum flux vector distributions and the depth-averaged velocity vector distributions under various discharge conditions are presented in **Figs. 27, 28,** and **29,** respectively. The features of flow fields obtained under each hydraulic condition are quite similar to each other, but quite different from those obtained in actual river channels. That is, the water surface elevations in **Fig. 27** are quite uniform in transverse direction. The momentum flux vector distributions, and the

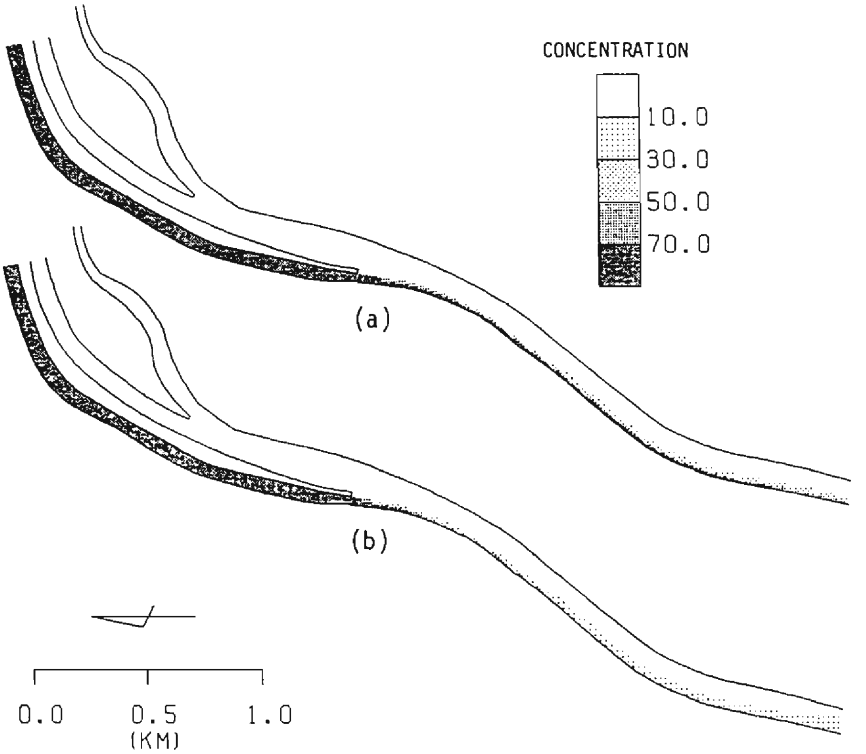

Fig. 25. Spreading of tracer concentration from the Katsura River in various channel geometry under the regime of 62–0904 Test for Model river (a), and Model river (b).

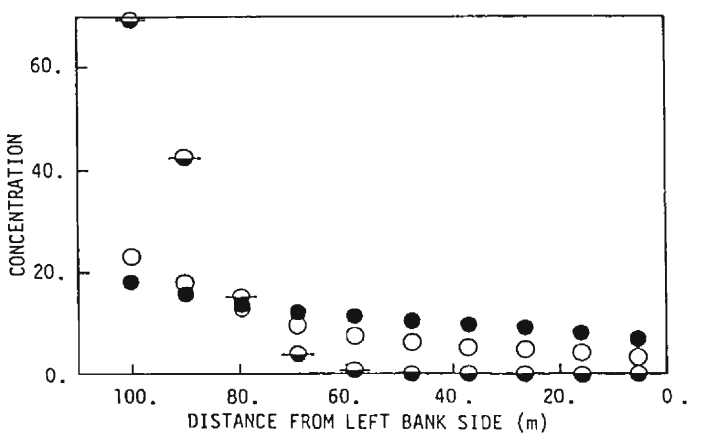

Fig. 26. Transverse distributions of tracer concentration at 33.6 km section in various channel geometries under the regime of 62 – 0904 Test. Solid circles denotes distributions for the actual river cross-section, half closed circles for model river (a), and open circles for model river (b).

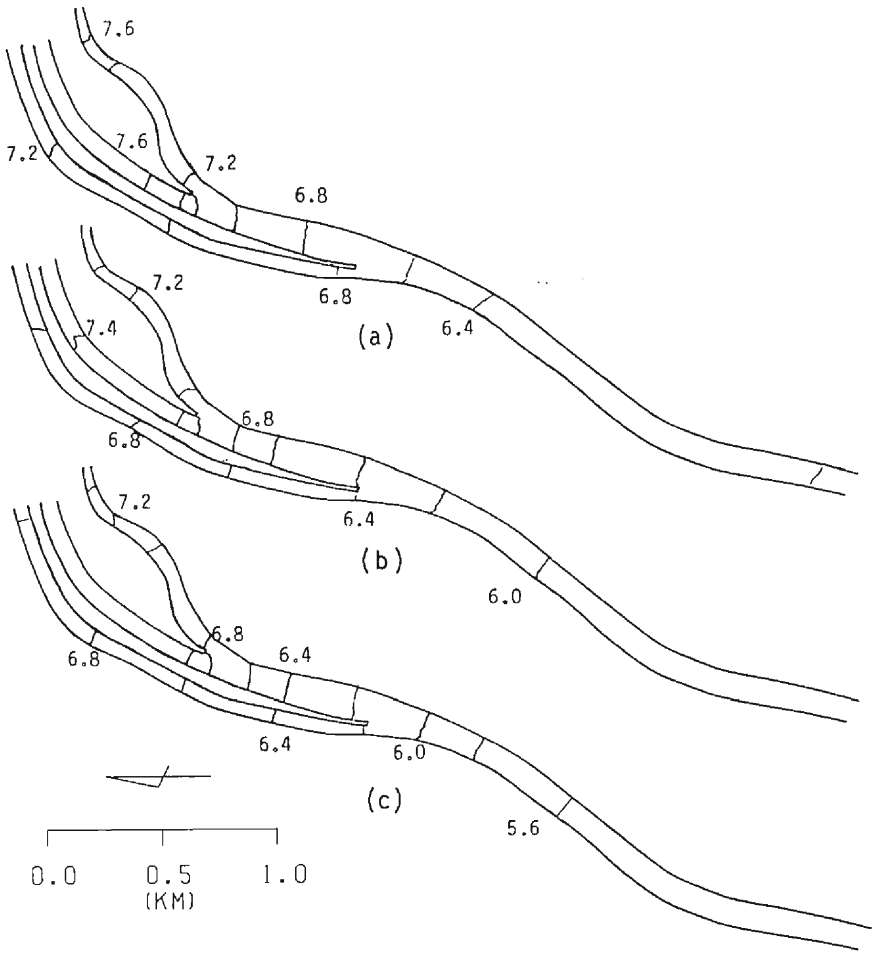

Fig. 27. Water surface elevation contour maps in rectangular crosssection channels under various flow regimes. (a) Ordinary (185-day) water discharge, (b) low water (275-day) discharge, and (c) drought (355-day) discharge.

depth-averaged velocity vector distributions are also quite uniform in the transverse direction except near the side-boundaries, and in the longitudinal direction, because the river bed elevation is uniform in the lateral direction.

(b) Concentration Distributions

The spreading of tracer concentration in various flow regimes is presented in **Figs. 30(a)**, **(b)**, and **(c)**. The transverse concentration distributions are also presented in **Figs. 31 (a)** and **(b)**.

Comparing the results in actual river channels presented in **Figs. 18** and **19**, the spreading width is controlled and limited and the concentration distributions are much less uniform, with only a little difference of concentration distributions among various

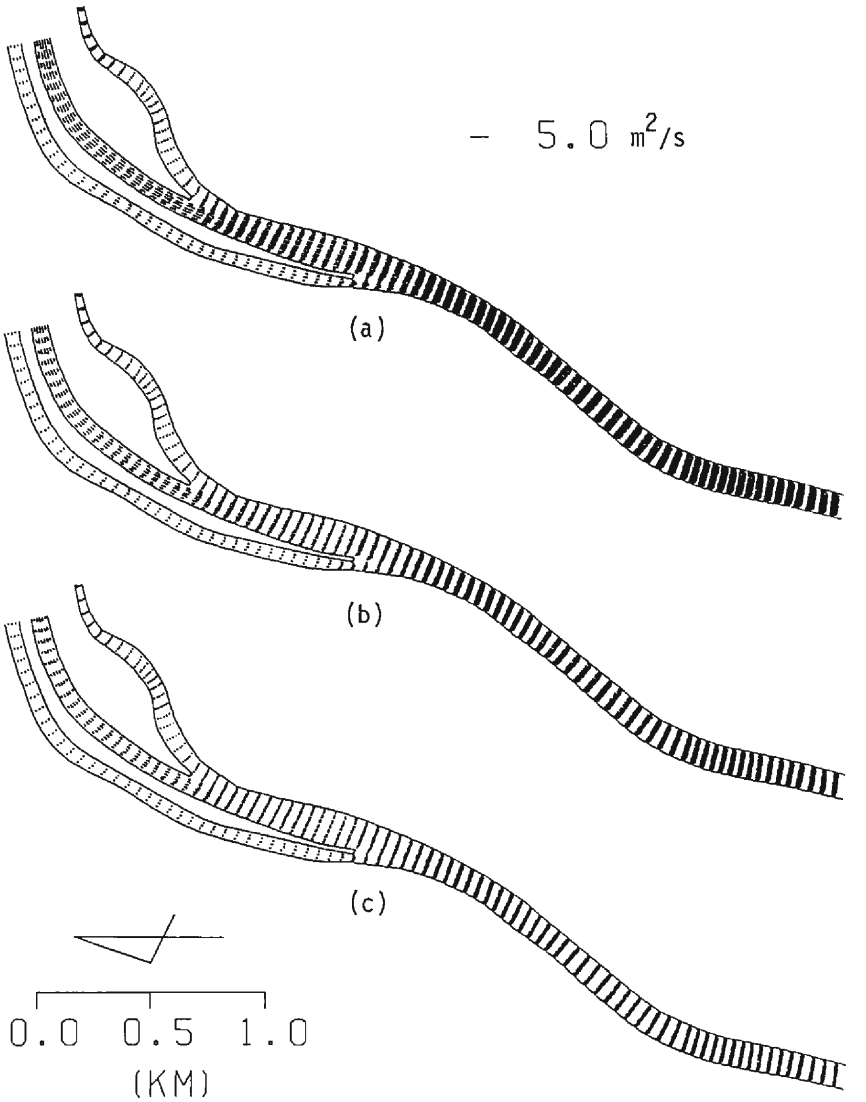

Fig. 28. Momentum flux vector distributions in rectangular cross-section channels under various flow regimes. (a) Ordinary (185-day) water discharge, (b) low water (275-day) discharge, and (c) drought (355-day) discharge.

flow regimes being observed. This is because the momentum flux vector distributions are uniform in the longitudinal direction as shown in **Fig. 29**, and, therefore, the convective transport in the transverse direction is very small and the mixing is mainly caused by transverse dispersion.

The transverse concentration distributions under various transverse dispersion coefficients in the regime of the low water discharge are presented in **Figs. 32(a)** and **(b)**. The

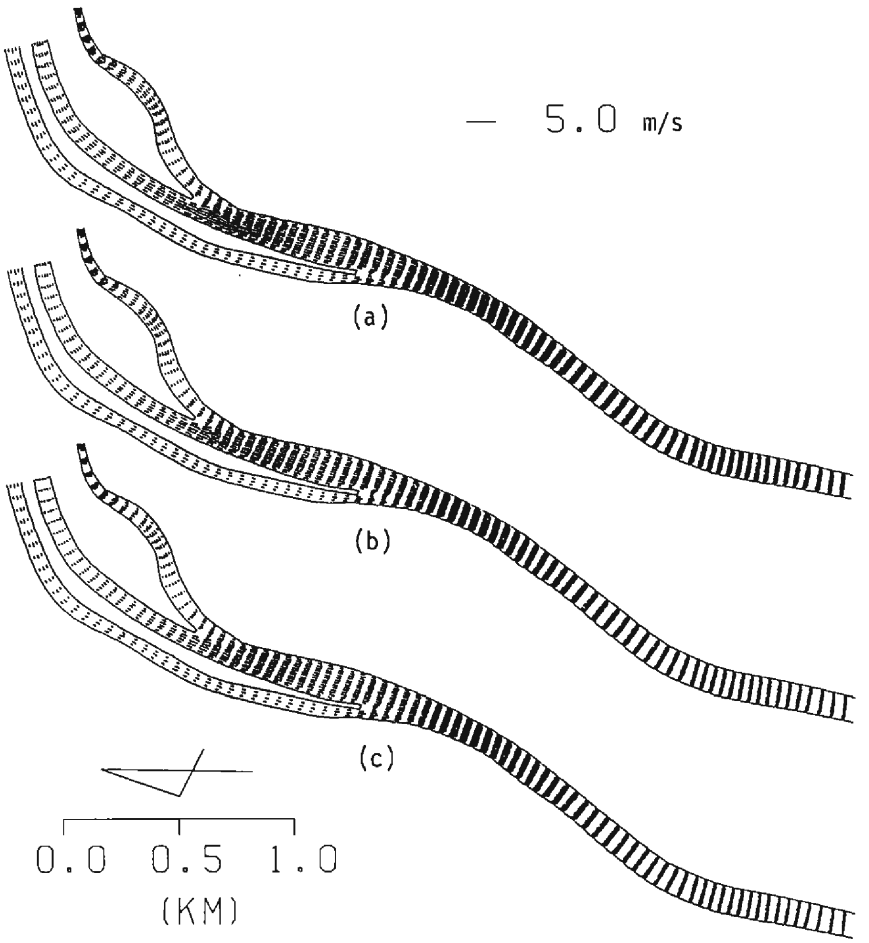

Fig. 29. Depth-averaged velocity vector distributions in rectangular cross-section channels under various flow regimes. (a) Ordinary (185-day) water discharge, (b) low water (275-day) discharge, and (c) drought (355-day) discharge.

results under the transverse dispersion coefficient of $\alpha_T = D_T/hu_* = 0.02$ and 0.2 are similar to each other at the 33.6km section and 32.08km section, but its effect is more obvious under the dispersion coefficient of $D_T/hu_* = 2.0$, and the high concentration at the right bank-side is lower.

Thus, transverse spreading is hardly affected by the flow regimes, but mainly governed by transverse dispersion transport because the river bed elevation is uniformly distributed. Furthermore, the momentum flux vector distributions are also uniform in the longitudinal direction, and the convective transport is minor. Therefore, the estimation of the magnitude of the transverse dispersion coefficient is more important in rectangular cross-section channels than in actual river channels.

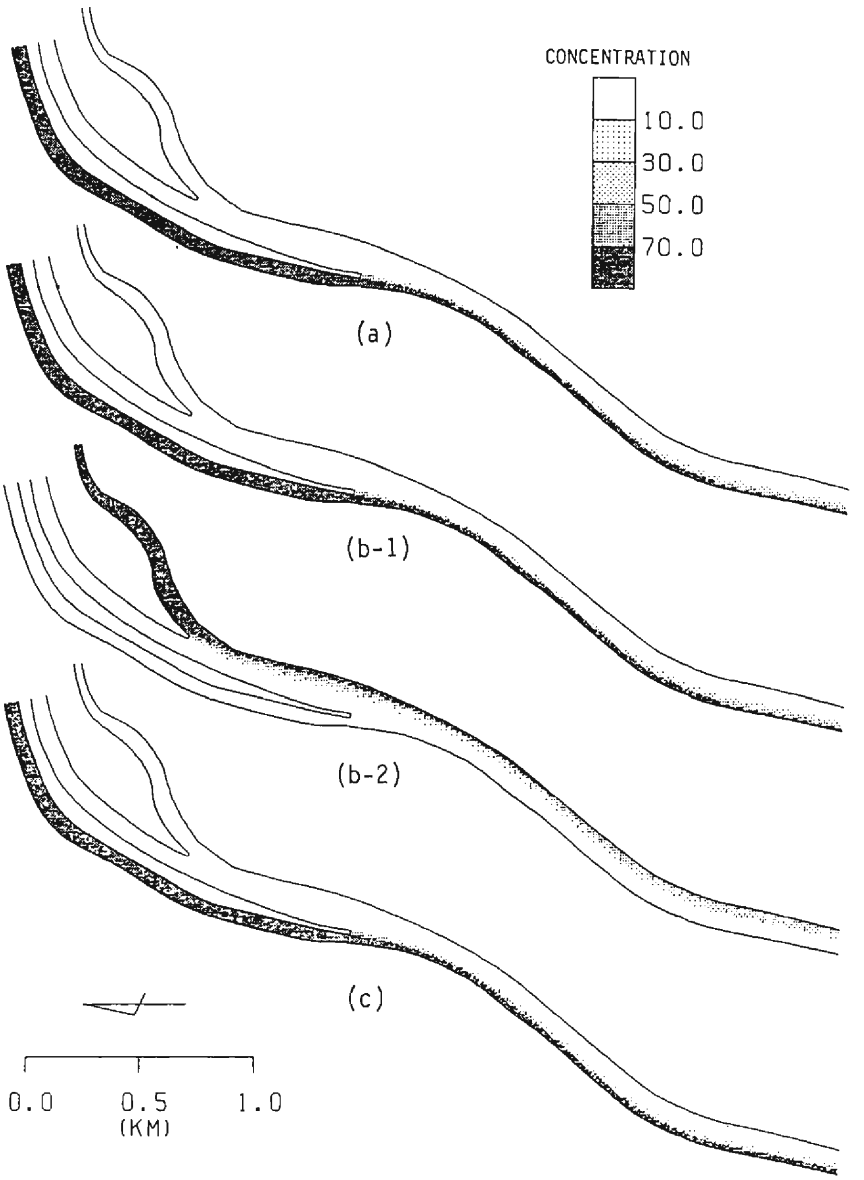

Fig. 30. Spreading of concentration in rectangular cross-section channels under various flow regimes. (a) Annual average discharge, (b) low water (275-day) discharge, and (c) drought (355-day) discharge.

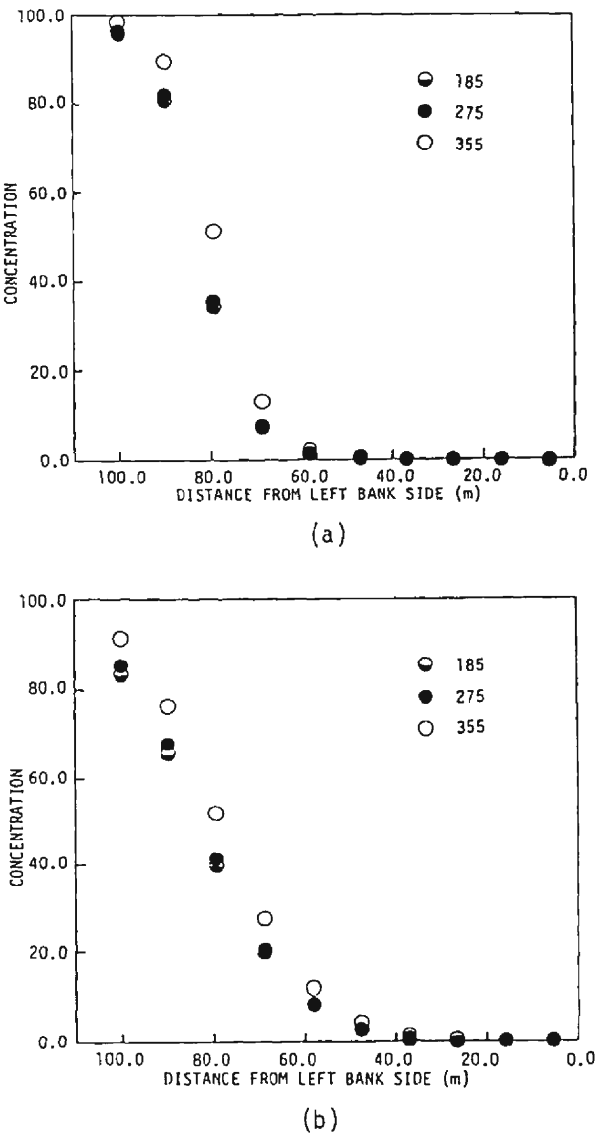

Fig. 31. Transverse distribution of tracer concentration in rectangular cross-section channels under various flow regimes for (a) 33.6km section, and (b) 32.05km section. Open circles denote the distribution for drought water (355-day) discharge, solid circles for low water (275-day) discharge and half-closed circles for ordinary (185-day) discharge.

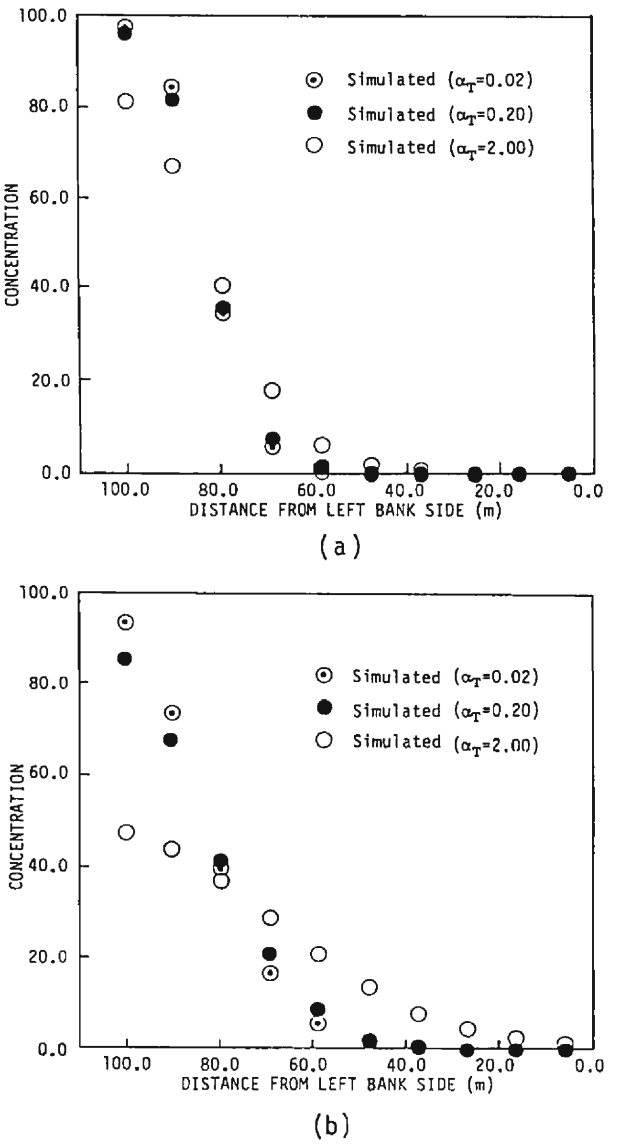

Fig. 32. Transverse concentration distributions under various transverse dispersion coefficients in Regime of the low water discharge for (a) 33.6km section, and (b) 32.08 km section. Circles with dot denote the results under the transverse dispersion coefficient of $D_T/hu_*=0.02$, solid circles under $D_T/hu_*=0.2$, and open circles under $D_T/hu_*=2.0$.

4.3 Laboratory Flume Experiment

(1) Simplified Hydraulic Model Experiment

A series of hydraulic experiments employing a laboratory flume was conducted in order to verify the characteristics of the mixing obtained in the numerical experiment. A

Table 3. Summary of conditions of simplified hydraulic model experiment

Run No.	Depth h(cm)	Discharge Q(l/s)	Velocity U(cm/s)	Flume
1	0.610	0.239	15.7	rectangular
2	0.696	0.263	15.1	simplified model
3	1.040	0.536	20.6	simplified model

straight flume, 25.0cm in width, had a series of rectangular shaped depressions on the bottom alternately located beside the right or left channel-side. Dimensions of a depression were 75.0cm long, 5.0cm wide and 1.0cm deep. This flume was used as a simplified hydraulic model of the Yodo River System below the confluence, and its scale is about 1/400 in the horizontal plane and 1/200 in the vertical direction. A rectangular cross-section channel was also used. The hydraulic conditions in the experiments are summarized in **Table 3** and the discharge in Run 1 is equivalent to annual average discharge in the prototype.

The dye-solution used as the tracer was continuously injected as a point source at the upstream section of the flume. The tracer spread in the transverse and the longitudinal directions and its dispersion cloud was observed and recorded by use of a photo-camera, but quantitative measurements were not made.

(2) Results and Discussions of the Hydraulic Experiment

The spreading of the tracer cloud observed in a rectangular cross-section flume test is illustrated in **Fig. 33** for (a) a rectangular cross-section flume test, and for (b), (c) and (d) a flume with depressions. The tracer injected near the channel-side spreads in the transverse direction in flowing down, but the width of the tracer cloud is smaller over depressions and larger below the end of the depressions. The transverse mixing was the largest in Run 2, second in Run 3 and third in Run 1, and these results are in accordance with the results obtained in numerical experiments. That is, the spreading width becomes larger as the discharge decreases in the channel with depressions, and it is the smallest in a rectangular cross-section channel. **Fig. 33(d)** shows the spreading of the tracer cloud injected at the half-width (the center of the flume). The meandering of the dye cloud suggests the flow also meanders and it is caused by the depressions; the flow accumulating over the depressions spreads in the transverse direction below their downstream end, where the flow depth becomes shallower, and the flow again converges and accumulates over them at each of their upstream ends. Thus, the spreading and convergence of flow caused by depressions accelerates the transverse mixing. This effect is stronger as discharge and/or average depth decreases as shown in **Figs. 33(b)** and **(c)**.

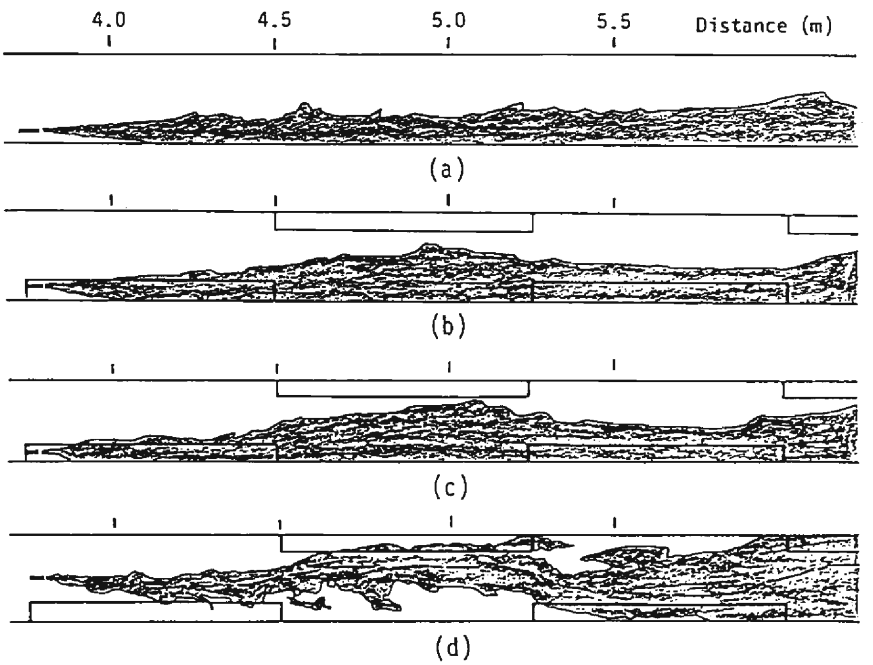

Fig. 33. Spreading of continuously injected dye solutions. (a) Run 1 : rectangular cross-section flumes, and side injection, (b) Run 3 : simplified model with depressions, and side injection, (c) Run 2 : simplified model with depressions, and side injection, and (d) Run 2 : simplified model with depressions, and center injection.

5 Conclusions

The 2-D mathematical models in the generalized curvilinear coordinate system were derived from common 2-D plain hydraulic models in the Cartesian coordinate system in **Section 2.** Their dependent variables are the same as those in the Cartesian coordinates system and only the independent variables are transformed into the non-orthogonal curvilinear system. The space coordinate system is non-orthogonal curvilinear system, with which it is much easier to generate the grids for calculation in the physical domain. The finite difference forms of the mathematical models in the curvilinear coordinate system were obtained by the integration method. They have second order accuracy in space and time coordinates. In addition, numerical models were also developed.

The proposed models were applied to the confluence of the Yodo River System case study and its validity was examined in **Section 3.** Although the simulated flow behavior was not compared with field data, the water surface elevation distributions, the momentum flux vector distributions and the depth-averaged velocity vector distributions simulated were reasonable and their features were discussed in detail with relation to channel bathymetry. It was disclosed that the water depth was shallow in low/drought

discharge conditions, and the flows in channels were much affected by the river bed elevation which is non-uniformly distributed in the longitudinal direction as well as the transverse direction. The simulated concentration distributions were successfully compared with the measured ones. The concentration distributions of contaminants were mostly affected by the convective transport of the flows, and the transverse mixing coefficient was estimated at less than $2.0hu_*$. The mixing processes of the waters from the Katsura River or the Kizu River below the confluences were also discussed in detail with their relation to the flow behavior.

The mechanism of the mixing in the Yodo River System was also investigated by the numerical experiments under various discharge conditions, dispersion coefficients, and channel geometries in **Section 4.** The features of the mixing processes in the Yodo River System disclosed by numerical experiments were summarized as:

1. The river bed in the Kizu River is the highest and that in the Uji River is the lowest in the lelvation, and the waters in the Kizu River and the Katsura River merge into the water in the Uji River at the confluences.
2. Below the confluence, the river bed is still not uniform, and the river mainly flows in the lower part of the river bed and the main water-stream changes its route from one side to the opposite side of channel in accordance with the non-uniform river bed topography. This meandering causes spreading and convergence of flows.
3. The spreading width of the tracer cloud changes in the longitudinal direction in accordance with the divergence and the convergence of flows, and transverse mixing is accelerated.
4. In case the total discharge is larger or the cross-section of channel is rectangular, the longitudinal variation of the transverse distribution of the momentum flux vectors is smaller and the transverse mixing is also smaller. Therefore a tracer cloud spreads more widely as total discharge is smaller in the actual river channel with non-uniform river bed distributions.

The features described above were also verified by simplified hydraulic experiments.

Thus, the transverse convective transport caused by the longitudinal variation of the transverse distributions of the momentum flux vector plays an important role in transverse mixing as well as the dispersive transport. This convective transport is more dominant than the turbulent and dispersive transport under the low flow condition in the actual river with non-uniform river bed elevation in both the longitudinal and the transverse directions. However, dispersive transport is more important in channels where there is no longitudinal variation of the river bed elevation and the momentum flux vector distributions.

The writers express their sincere appreciation to the graduate and undergraduate students in River Hydraulics Laboratory, Faculty of Engineering, Kyoto University for their kind help in performing the numerical experiment, and preparing drawings.

References

1) Yotsukura, N. and W. W. Sayre: Transverse mixing in natural streams, *Water Resources Research,* Vol. 12, No. 4, 1976, pp. 695–704.
2) Lau, L. and B. G. Krishnappan: Modeling transverse mixing in natural streams, *Proc. ASCE,* Vol. 107, No. HY2, 1981, pp. 209–226.
3) Holly Jr., F. M. and G. Nerata: Field calibration of stream-tube dispersion model, *Proc. ASCE,* Vol. 109, No. HY11, 1983, pp. 1455–1470.
4) Li, S., S. Yagi and T. Sueishi: Transverse dispersion of water quality in the Yodo River and its effect on the source of water supply. *Proc. 31st Japanese Conference on Hydraulics,* JSCE, 1987, pp. 311–316 (in Japanese).
5) Viviand, H.: Formes conservatives des equations de la dynamique des gaz, *La Recherche Aérospatiale,* No. 1, 1974, pp. 65–66.
6) Leonard, B. P.: A stable and accurate convective modelling procedure based on quadratic interpolation, *J. Computational Methods in Applied Mechanics and Engineering,* No. 19, 1979, pp. 59–98.
7) Takemoto, et al.: A curvilinear coordinate method for the solution of incompressive Navier–Stokes equations using the third-order upwind difference scheme, Transaction of JSIDRE, No. 121, 1986, pp. 57–65.
8) Kawamura, T.: Direct simulation of flows at high Reynolds number using a third-order upwind scheme, in "Recent studies on turbulent phenomena" edited by Tatsumi, T. et al, Assoc. Science Documents Information, Tokyo, 1985, pp. 117–149.
9) Iwasa. Y., S. Aya, T. Tsuchiya and Y. Nishiuchi: 2-D numerical simulation of flow and associated dispersion by means of generalized curvilinear coordinate system, *Annuals,* Disaster Prevention Research Institute, Kyoto University, Vol. 31, B-2, 1988, pp. 589–600 (in Japanese).
10) Akima, H.: A new method of interpolation and smooth curve fitting based on local procedure, *J. Assoc. Computational Machinery,* Vol. 17, No. 4, 1970, pp. 589–602.
11) Elder, J. W.: The dispersion of marked fluid in turbulent shear flow, *J. Fluid Mechanics,* Vol. 5, 1959, pp. 544–560.
12) Okoye, J. K.: Characteristics of transverse mixing in open-channel flows, Report No. KH-R-23, California Institute of Technology, Pasadena, California, 1970.
13) Iwasa. Y., T. Hosoda, and Y. Noguchi: Transverse mixing coefficient in open-channel flows, *Annuals,* Disaster Prevention Research Institute, Kyoto University, Vol. 25, B-2, 1982, pp. 557–572 (in Japanese).
14) Webel, G. and M. Schuzmann: Transverse mixing in open channel flows, *Proc. ASCE,* Vol. 107, No. HY4, 1988, pp. 209–226.
15) Fischer, H. B. et al: Mixing in Inland and Coastal Waters, Academic Press, New York, 1979.
16) Iwasa, Y. and S. Aya: Spreading of effluent in receiving river waters, *Proc. 5th Int'l Conference on Urban Storm Drainage,* Vol. 1, 1990, pp. 541–546.
17) Oue, M., Y. Iwasa and S. Aya: Numerical experiments of flows and mixing at a confluence, *Proc. Annual Conference of JSCE,* Vol. 2, 1990, pp. 456–457 (in Japanese).
18) Yotsukura, N., H. Fischer and W. W. Sayre: Mixing characteristics of the Missouri river between Sioux city Iowa, and Plattsmouth Nebraska, Water-supply paper, 1899-G, U. S. Geological Survey, 1970.
19) Yotsukura, N., and S. Nakamura: The stream-tube model for the transport of dissolved materials in natural rivers, *Proc. JSCE,* No. 399, II-10, 1988, pp. 85–94 (in Japanese).
20) Holly Jr., F. M.: Dispersion in rivers and coastal waters— 1. Physical principles and disperion equations in "Developments in Hydraulic Engineering—3" edited by Novak, P., Elsevier, London, 1985.
21) Nambu, S.: Analysis of concentration distribution of contaminants in a polluted river, *J. Water Supply Eng. Assoc.,* No. 304, 1960, pp. 29–37 (in Japanese).
22) Yoneda, N., K. Iwata and Y. Inoue: Estimation of transverse dispersion coefficient by use of water quality data measured in a river, *Proc. 8th Kyoto Univ. Symposium on Environmental Engineering,* 1986, pp. 103–110 (in Japanese).